Fusion Engineering and Design 217 (2025) 115133

Contents lists available at ScienceDirect

Fusion Engineering and Design

journal homepage: www.elsevier.com/locate/fusengdes

Overview of deuterium-tritium nuclear operations at JET

R. Villari [a,*], X. Litaudon [b], J. Mailloux [c], M. Dentan [b,s], N. Fonnesu [a], Z. Ghani [c], L.W. Packer [c], F. Rimini [c], R. Vila [d], R. Afanasenko [j], J. Alguacil [f], P. Batistoni [a], P. Beaumont [c], S.C. Bradnam [c], P. Carman [c], J.P. Catalan [f], M. Cecchetto [s], A. Colangeli [a], D. Croft [c], J. Cufe [n], M. De Pietri [f], M. Fabbri [q], J. Figueiredo [k,l], D. Flammini [a], C.L. Grove [c], A. Hjalmarsson [m], V. Ioannou-Sougleridis [g], L. Jones [c], R. Kierepko [i], M. Klosowski [i], A. Kolsek [q], B. Kos [e,m], E. Laszynska [h], E. Lerche [c,o], Y. Le Tonqueze [r], D. Leichtle [j], E. Leon-Gutierrez [d], I. Lengar [e], M. Loughlin [p], R. Lobel [c], S. Loreti [a], G. Mariano [r], S. Mianowski [c], J. Milnes [c], S. Moindjie [t], F. Moro [a], J. Mietelski [i], R. Naish [c], S. Noce [a], J. Peric [e], J.B. Pontier [n], S. Reynolds [c], V. Radulović [e], M.I. Savva [g], P. Sauvan [f], C.R. Shand [c], L. Snoj [e], I.E. Stamatelatos [g], Z. Štancar [c], T. Stokes [c], N. Terranova [a], A.N. Turner [c], T. Vasilopoulou [g], A. Wójcik-Gargula [i], the JET contributors [1]

[a] ENEA, NUC Department, Via E. Fermi 45, 00044 Frascati, Rome, Italy
[b] CEA, IRFM, F-13108 St-Paul-Lez-Durance, France
[c] UK Atomic Energy Authority, Culham Campus, Abingdon, Oxon, OX14 3DB, UK
[d] Laboratorio Nacional de Fusión, CIEMAT, Av. Complutense, 40, 28040 Madrid, Spain
[e] Reactor Physics Department, Jožef Stefan Institute, Jamova cesta 39, 1000 Ljubljana, Slovenia
[f] Universidad Nacional de Educación a Distancia (UNED), C/Juan del Rosal 12, Madrid, Spain
[g] National Centre for Scientific Research Demokritos, Athens, Greece
[h] Institute of Plasma Physics and Laser Microfusion, Hery Street 23, 01-497 Warsaw, Poland
[i] Institute of Nuclear Physics Polish Academy of Sciences, ul. Radzikowskiego 152, 31-342 Krakow, Poland
[j] Karlsruhe Institute of Technology, 76344 Eggenstein-Leopoldshafen, Karlsruhe, Germany
[k] EUROfusion Programme Management Unit, Garching, Germany
[l] Instituto de Plasmas e Fusão Nuclear, Instituto Superior Técnico, Universidade de Lisboa, Lisboa, Portugal
[m] Department of Physics and Astronomy, Uppsala University, Sweden
[n] CEA, DES/ISAS/SERMA, F-91191 Gif-sur-Yvette, France
[o] Laboratory for Plasma Physics, Ecole Royale Militaire, Brussels, Belgium
[p] Oak Ridge National Laboratory, 1 Bethel Valley Road, Oak Ridge, TN, 37831, USA
[q] Fusion for Energy, Josep Pla 2, Barcelona, 08019, Spain
[r] ITER Organization, Route de Vinon-sur-Verdon - CS 90 046 - 13067 St Paul Lez Durance Cedex. France
[s] CERN, CH-1211 Genève, Switzerland
[t] Aix-Marseille University, CNRS, IM2NP (UMR 7334), F-13397 Marseille Cedex 20, France

ARTICLE INFO

Keywords:
Neutronics
JET
DT
Benchmark
Activation
SEE

Two unique high-performance Deuterium-Tritium (DT) campaigns were performed at JET in 2021 and 2023 producing more than $1.5{\cdot}10^{21}$ 14.1 MeV neutrons. These campaigns not only achieved breakthroughs in fusion energy but also provided unique opportunities for integrated testing of a nuclear tokamak operation in DT. An outstanding amount of nuclear fusion-related data has been collected through EUROfusion technological exploitation of JET DT operations. Started within the JET3 project and continuing in the 'Preparation of ITER Operations' (PrIO) work-package, the experiments aimed to enhance nuclear technology understanding, validate codes and data, and optimize nuclear operations at ITER. Neutronics experiments explored activation of real ITER materials, damage to functional materials, water activation in a tokamak cooling loop, and effects on electronics. Benchmark experiments validated computational tools and nuclear data for ITER nuclear analyses. The acquired experience is crucial for ITER nuclear phase, safety demonstrations, and DT-2 licensing, making the

* Corresponding author.
E-mail address: rosaria.villari@enea.it (R. Villari).
[1] See the author list of "'Overview of T and D-T results in JET with ITER-like wall" by CF Maggi et al. 2024 Nucl. Fusion 64 112012

https://doi.org/10.1016/j.fusengdes.2025.115133
Received 8 December 2024; Received in revised form 22 March 2025; Accepted 25 April 2025
Available online 13 May 2025

JET DT results highly valuable for ITER program advancement. The paper provides a comprehensive overview of activities, emphasizing key findings, achievements, lessons learned so far, issues, and outcomes for the ITER program, licensing, and nuclear operations.

1. Introduction

The recent and successful Deuterium-Tritium experimental (DTE) campaigns at the Joint European Torus (JET) marked significant progress in fusion energy development. In 2023, a new fusion energy record of 69 MJ [1] was achieved, surpassing the previous record of 59 MJ set in 2021 [2]. These campaigns not only achieved breakthroughs in fusion energy but also allows for advancing in plasma physics understanding of impact of isotope mass on plasma confinement, transport from the core to the edge, plasma-wall interaction, alfa-particle heating, etc. [1–4].

From the technology perspective, these experiments provided unique opportunities for gaining operational experience, gathering information on the tritium fuel cycle and fuel retention and for integrated testing of a nuclear tokamak operation in DT, essential for advancing to the next generation of fusion machine like ITER and DEMO.

The EUROfusion technological exploitation of JET DT operations, started within the JET3 project [5] and continued under the 'Preparation of ITER Operations' (PrIO) work-package [6] since 2020, gathers unique nuclear fusion-related data yielding substantial insights and outcomes. Many technology-oriented experiments were conducted in DT aimed at enhancing the knowledge of nuclear technology and safety, develop and validate nuclear codes in a complex environment, data, methodologies and experimental techniques in preparation of ITER nuclear operations [6].

The project comprises neutron activation measurements and analysis of real ITER materials, irradiation of functional materials for damage studies, neutron streaming and shutdown dose rate (SDDR) benchmark experiments. It also includes procedure for the 14 MeV neutron diagnostics calibration, tests of detectors for Test Blanket Module (TBM), assessment of advanced neutron shield performance and collection of Occupational Radiation Exposure (ORE) and nuclear waste data. Advancements in nuclear code development, integrated neutron source modeling, and experimental technique refinement were also accomplished. Furthermore, unique experiments were conducted to study complex and important phenomena such as water activation in a real JET cooling loop and Single Events Effects (SEE) induced by neutrons on electronics, correlating them with plasma DT operations. These experiments provide essential outcomes for evaluating computational reliability, enhancing design, and optimizing safety.

The JET DT results are particularly crucial now for providing inputs to the ITER nuclear phase and safety demonstrations, especially as the ITER Organization proposes a revised timeline with an accelerated approach to nuclear operations once the construction is complete [7].

The present paper provides an overview of the technology-oriented experiments performed during DT operations at JET. Analyses of the experiments are still in progress and dedicated papers will follow.

A summary of DT nuclear operations with focus on neutron production is in Section 2. The neutron irradiation conditions at JET are compared with those expected in ITER in Section 3. Section 4 is dedicated to the technological exploitation of DT operations including an overview of activities, emphasizing key findings, achievements, lessons learned so far, issues, and preliminary outcomes for the ITER program, licensing, and nuclear operations.

2. DT operations at JET and neutron production

Nowadays, most of the fusion devices operate with hydrogen and deuterium. DT operations in tokamaks were performed only at JET in UK and at Tokamak Fusion Test Reactor (TFTR) in US. The time evolutions of the fusion power for the most significant scenarios for TFTR and JET in DT are shown in Fig. 1 [3]. The first demonstration of the feasibility of DT operations in a tokamak occurred in 1991 with the PTE1 experiment at JET, using 10% of T in D-T mixture [8]. DT campaigns were performed at TFTR in 1994–1996 using 90 g of tritium [9]. These experiments demonstrated the viability of 50:50 DT mixture operations, provided the first measurements of alpha heating and transport, Ion Cyclotron Radio Frequency (ICRF) heating and current drive of DT plasmas. A 10.7 MW fusion power record was achieved ($Q = 0.27$), even if only for short time [9]. TFTR machine was closed in 1997. In the same year, the first extensive use of tritium was carried out at JET with the Deuterium-Tritium Experiment 1 (DTE1) [10,11]. Various DT mixtures were tested and compared, the record fusion power performance in both transient (16 MW, $Q = 0.62$) and steady operations (4 MW) was achieved and several physics studies were performed using 99.3 g of tritium. Later on, a trace tritium experiment (TTE) was performed in JET in 2003 to study the physics of thermal and fast particle transport in various scenarios, heating and current drive using low tritium concentrations (up to 3%) [12]. Very high tritium retention was found with carbon-wall [13], driving the replacement of the plasma facing components with Be in the first wall and W in the divertor, referred as to the ITER like-wall (ILW). The ILW installation was performed in the years 2009–2011 [14]. A high performance DT experiment, Deuterium-Tritium Experiment-2 (DTE2), with a neutron budget of 1.7×10^{21}, 7 times higher that all previous campaigns with tritium, was planned to perform experiments in conditions as close as possible to those foreseen for ITER and thus provide the best possible preparation and training [15].

After several years with extensive preparatory activities in the previous deuterium campaigns and numerous enhancements (new fusion diagnostics, new T injection capabilities, refurbishment of the T plant, increased auxiliary heating, in-vessel calibration of 14 MeV neutron yield monitors, advances in plasma theory and modelling) [16], a

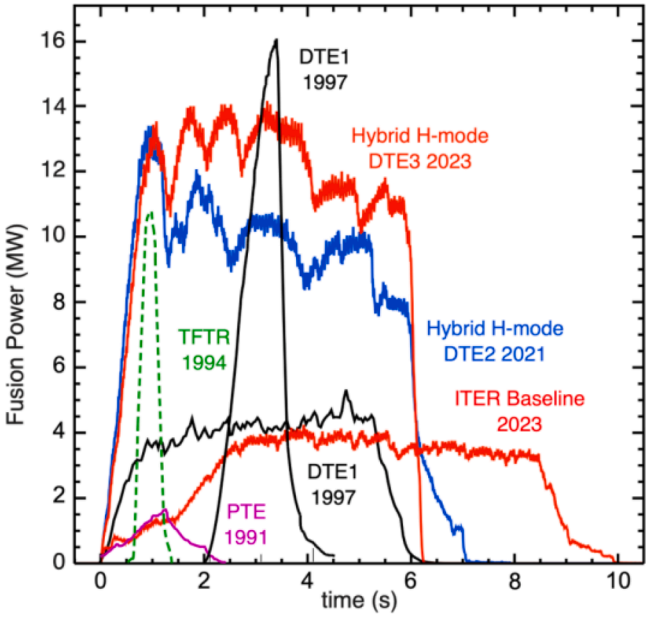

Fig. 1. Fusion power for relevant DT pulses of JET in PTE1; DTE1 fusion power record #42,976 and stationary #42,982; DTE2 prior fusion energy record #99,971; and DTE3 fusion energy record pulse # 104,522 and ITER baseline # 104,600. TFTR former fusion power record is also shown. Figure reproduced from [3].

successful DTE2 experiment was performed in 2021, demonstrating DT operations with metal wall ([2,3]). About 1 kg of tritium was used, yielding DT fusion reactor relevant plasmas to date and expanding the understanding of isotopes and D-T mixture physics. During DTE2, 8.48 $\times$ 10^{20} DT neutrons were produced.

With the T-rich (with 15% D and 85% T) hybrid scenario the highest sustained D-T fusion performance were achieved, establishing a record of 59 MJ fusion energy. Tritium-Tritium (TT) operations were performed before and at the end of DTE2 and a long lasting DD campaign followed. The DTE3 campaign [1] hold on in 2023, focused on developing scenarios for ITER and DEMO and real-time control techniques, perform tritium retention and clean-up studies, and complement technological exploitation with ITER relevant experiments on water activation and single-event effects on electronics. In DTE3, ~117 *g* of tritium were supplied to the Tritium Introduction Modules (TIMs) (only deuterium NBI was used) and a total of 7.31 $\times$ 10^{20} DT neutrons were produced. Improving the stationarity of the high performance hybrid scenario, through the optimization of the plasma composition and heating methods, it was possible to reach an higher fusion energy record of 69 MJ with T-rich plasma and to develop a successful radiative Ne-seeded ITER baseline scenario.

Concerning neutron production, JET generated 1.57 $\times$ 10^{21} DT neutrons during DTE2 and DTE3. The total neutron yield per shot during 2021–2023 JET DD, TT and DT campaigns is shown in Fig. 2, the neutron yield from D-T reactions (i.e. 14 MeV neutron component) is also displayed separately [17]. Typically in pure DD plasma at JET the DT component is about 1% of the total neutron yield due to triton burn-up [18]. Due to D contamination in TT plasma and residual T during DD plasma operations following DT and TT campaigns, the percentage of neutron produced from DT reactions varies along the operations and tritium retention plays a role too [17]. In TT campaigns the total neutron production from D-T reactions is approximately 40% (the remainder is from T-T reactions). At the end of DTE3, the contribution of the 14 MeV neutron component decreases to a few percent at the end of operations, thanks to a successful clean-up, optimized on the basis of DTE2 experience [19].

A large number of pulses in DTE2 and DTE3 campaigns have high neutron production with many shot at neutron yield rate greater than 10^{18} n/s, i.e. approximately two orders of magnitude higher than DD and TT operations. In the highest performances, for the record pulse #104522, 2.46 $\times$ 10^{19} neutrons were produced over about 6 s with a neutron yield rate peak of 5.06 $\times$ 10^{18} n/s (see Fig. 3).

3. Relevancy for ITER nuclear technology

According to the recent re-baselining under development, ITER is

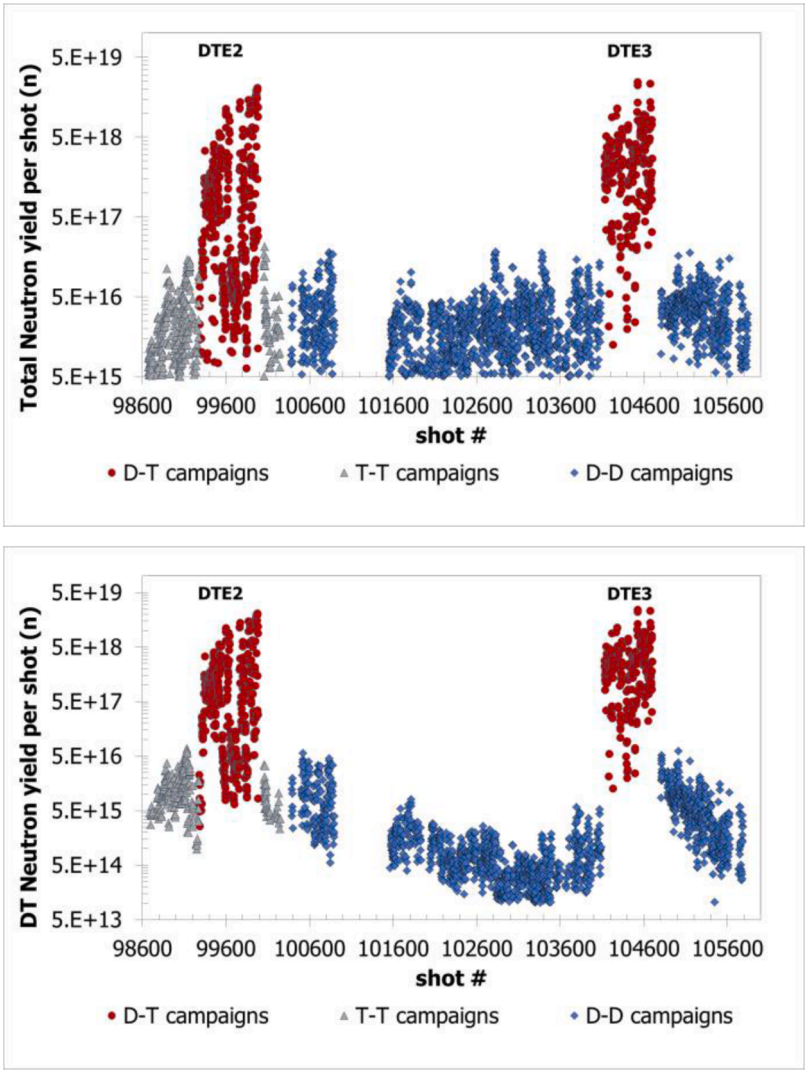

Fig. 2. Total neutron yield per shot (top) and DT component (bottom) neutron yield in the JET DD, TT and DT campaigns over the last 3 years of operations. Only the pulses with total neutron yield greater than 5 $\times$ 10^{15} n are shown.

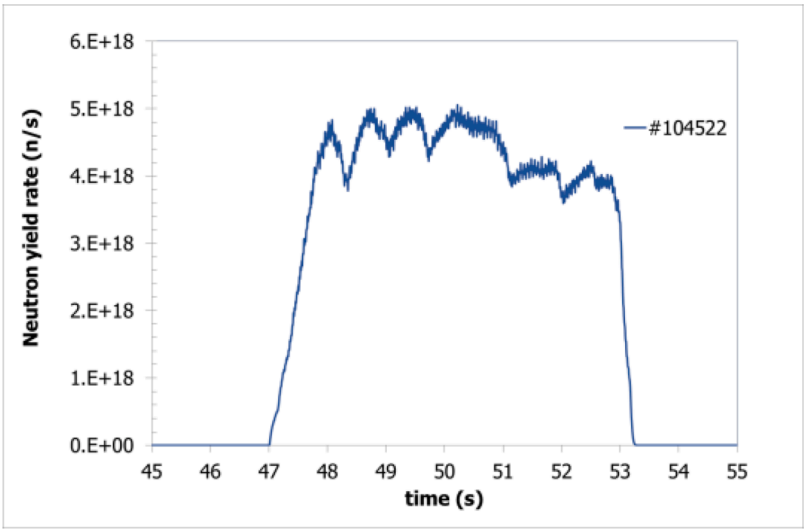

Fig. 3. Neutron yield rate versus time of the fusion energy record pulse #104522 from the time resolved neutron yield monitors (KN1).

expected to produce at the end of the first phase of operations in DT, i.e. DT-1, 3×10^{25} neutrons, that represents 1% of its lifetime, corresponding to 3×10^{27} neutrons (i.e. at the end of DT-2) [7].

JET generated during DTE2 and DTE3 campaigns a total of 1.57×10^{21} neutrons, accounting for 80% of the total DT neutron production by JET over the past 40 years, which is 1.83×10^{21} n. When comparing the total neutron yield, the neutron production over ITER lifetime is 1.64×10^{6} times greater than that of JET entire operational life, or approximately 1.91×10^{6} times greater for DTE2 and DTE3 campaigns only. By the end of ITER DT-1 phase, the ratio decreases to 1.64×10^{4} relative to JET lifetime (1.91×10^{4} when considering only JET DTE2 and DTE3 campaigns). Thus, in terms of total neutron production, JET conditions are still very far from expected ITER.

Concerning the peak of neutron yield rates, JET achieved in 2023 a maximum rate of 5×10^{18} n/s (14 MW fusion power peak), while ITER is expected to reach a rate of 1.77×10^{20} n/s for 500 MW pulse. This results in a neutron yield rate ratio of approximately 35 between ITER and JET.

When considering neutron transport and interactions, due to its smaller size relative to ITER, JET shows a neutron flux through its plasma-facing components of the order of 2×10^{13} n/cm^2/s at 14 MW, whereas in ITER first-wall, the neutron flux is approximately 2×10^{14} n/cm^2/s at 500 MW, covering a wide energy spectrum from thermal energies up to around 16 MeV. Therefore, in terms of neutron flux, JET peak conditions are only about one order of magnitude lower than that of ITER. The representativeness of JET conditions for ITER is evident from neutron flux spatial distributions. Neutron flux maps (in n/cm^2/s) in Fig. 4 shows the poloidal sections in JET octant 1 for a peak 14 MW pulse and in ITER Equatorial Port 12 [20] for 500 MW pulse, calculated using the MCNP5 radiation transport code [21].

Over the DTE2 and DTE3 campaigns, the cumulated neutron fluence on JET plasma-facing components reaches a level of 10^{16} n/cm^2. By comparison, the expected neutron fluence on ITER's first wall reaches approximately 10^{19} n/cm^2 by the end of DT-1 and 10^{21} n/cm^2 by the end of its life (DT-2). Though the neutron energy spectra will be different, a fluence of the level of 10^{16} n/cm^2 is expected in ITER in the middle port plugs and rear blanket areas by the end of DT-1 and in rear port plugs at the end of DT-2.

Therefore, the irradiation conditions achieved during JET DTE2 and DTE3 campaigns are highly relevant for ITER and future fusion reactor technologies. These conditions align well, in a stepladder approach, with those expected in ITER.

4. Technological exploitation of DT operations

The preparation of technological exploitation of DT operations started several years ago within JET3 [5] program and it was continued and expanded under WPPrIO [6], the work-package devoted to the EUROfusion contribution to the preparation of ITER operation and scientific exploitation. WP PrIO covers research, development, and validation on existing EU facilities of the scientific and operational tools to be compliant with ITER requirements and fully ready for preparing ITER operation.

The JET-related activities are carried-out in the frame of PrIO subproject 5 "Neutronics, Nuclear Waste and Safety", in which several European laboratories are conducting Research and Development (R&D) activities aimed at improving the knowledge of nuclear technology and safety, to develop and validate nuclear codes, neutronic tools and experimental techniques and to reduce the risks to ITER nuclear operations and maintenance activities. External international collaboration with ORNL in US has been established.

In particular, the JET technology-oriented experiments and analyses are carried-out in the frame of the sub-projects listed in Table 1, focused to:

- implement and validate methodology for 14 MeV neutron calibration;
- study activation and damage of materials, water and electronics;
- test Tritium breeding and TBM detectors;
- benchmark nuclear codes;
- develop and test advanced nuclear experimental techniques;
- collect and process nuclear safety data.

Several dedicated detection systems and samples were installed at JET, most of them already used in the previous DD and TT campaigns and integrated into JET Control and Data Acquisition System (CODAS). Water activation and neutron-induced Single Event Effect (SEE) experiments on electronics have been performed solely during DTE3.

The following sections present an overview of the experiments focused on nuclear technology under NC-14, ACT, RADA, NEXP, TBMD, WACT and SEE sub-projects as defined in Table 1. The safety-related activities concerning occupational radiation exposure, waste production, and characterization will be addressed in future publications.

4.1. Verification of 14 MeV neutron detector calibration methodology

Neutron diagnostics are fundamental in ITER for the assessment of

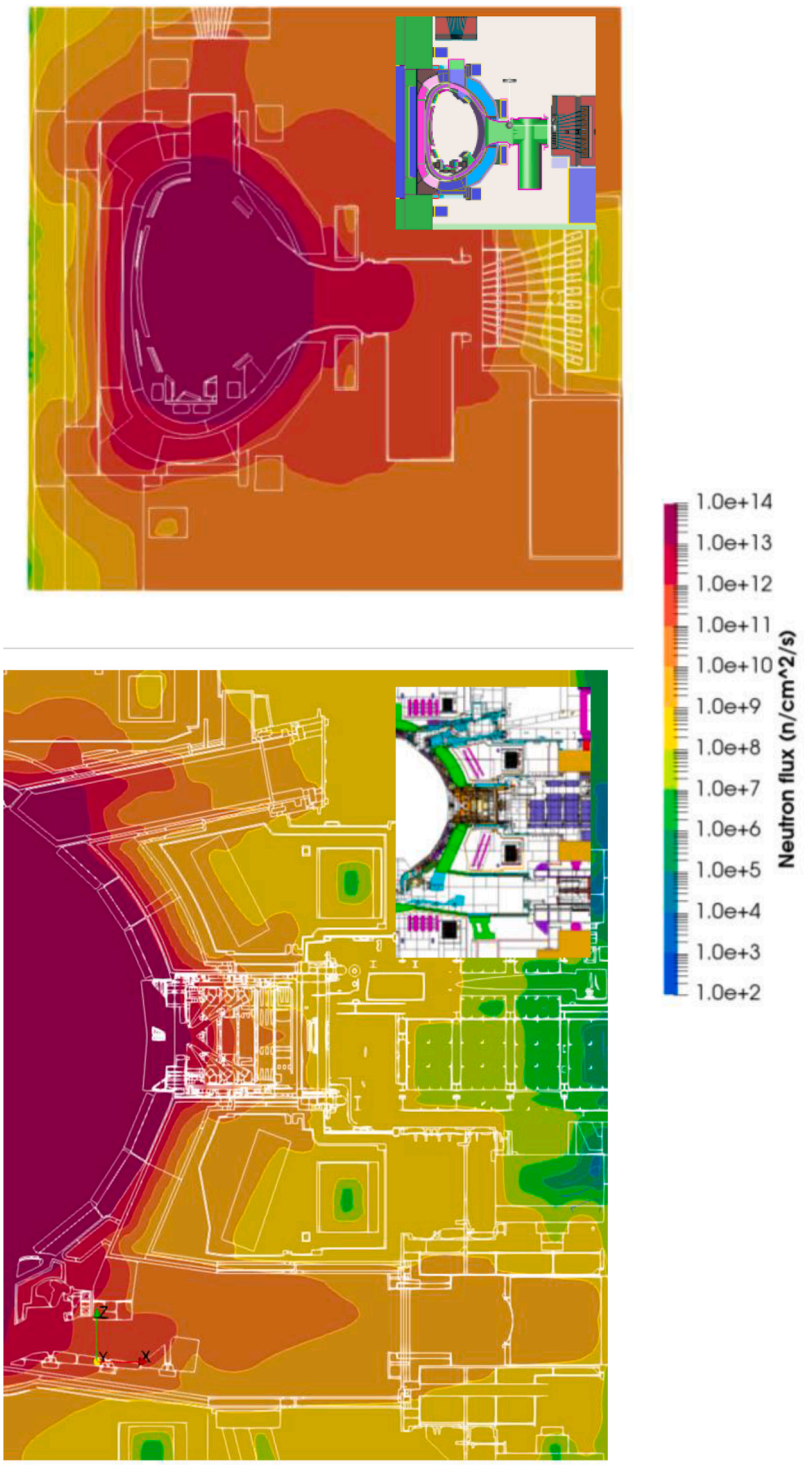

Fig. 4. Poloidal section of neutron flux maps calculated in the middle of JET octant 1 for 14 MW peak plasma conditions (top) and in the ITER C-model in the middle of Equatorial Port #12 [20] for 500 MW pulse.

the fusion performance and key plasma parameters. In particular, the demonstration of accuracy and reliability of the diagnostics used to measure fusion power will be crucial for obtaining approval for tritium operations in ITER and challenging calibration accuracy within ±10% is required [22].

In 2017, a novel 14 MeV neutron calibration was conducted at JET in preparation for DT operations [23,24], in the frame of EUROfusion WPJET3 project. The objectives were to allow accurate measurement of fusion power; reduce the uncertainties in the neutron yield compared to the allowed neutron budget and thus maximizing the scientific return of DT operations; minimize the uncertainties in neutronics benchmark experiments as well as gain experience for the future ITER neutron calibration.

A 14 MeV neutron generator (NG) with an intensity of $\sim 2 \times 10^8$ n/s, with its power supply and control unit was deployed inside the vacuum vessel using the JET Remote Handling (RH) boom and the MASCOT (MAnipolatore Servo COntrollato Transistorizzato) robotic arm (Fig. 5) [23,24]. The NG was equipped with two calibrated diamond detectors,

Table 1
Sub-projects of technological exploitation of DT operations at JET within EUROfusion JET3 2014–2020 and PrIO-SP5 2021–2025. Locations of the detectors/samples inside and ouside TH and CODAS integration.

Sub-Project	DD, TT, DTE2 Campaigns	DTE3 Campaign	Location of detectors /samples in Torus Hall	Location of detectors /samples in the Basement	CODAS
NC-14 14 MeV Neutron calibration	x	x	JET main neutron diagnostics KN1 (fission chambers) and KN2 (activation foils)		x
ACT Activation of ITER materials	x	x	Long Term Irradiation Station (LTIS) and Irradiation End		
RADA Radiation damage studies	x	x	LTIS		x
NEXP Streaming & Shutdown dose rate benchmark exp	x	x	several positions	various positions South-West labirinth & South-East chimney + pit	x
TBMD Test Blanket Module detectors - TBR	x	x	Octant 8, Octant 3 and Irradiation End		x
WACT* Water activation exp		x		Oct 4 basement	x
SEE* Single Event Effects on electronics		x		South-East basement	x
ORE Occupational Radiation Exposure	x	x			
WPC Waste production and characterisation	x	x			

* *New within PrIO*

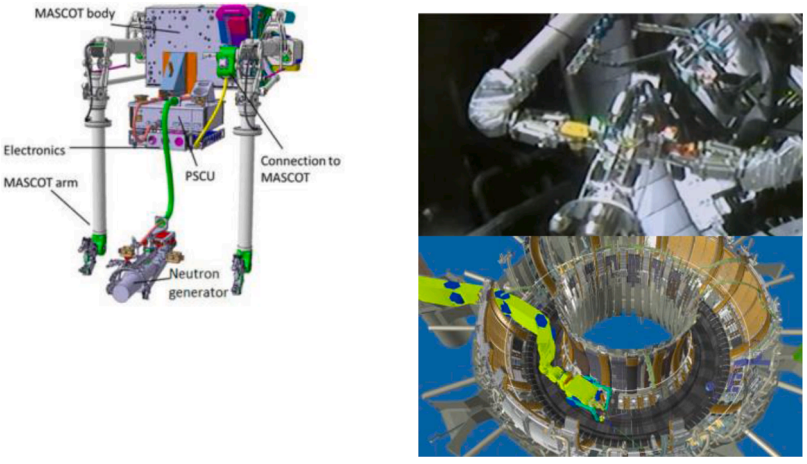

Fig. 5. The NG and the power supply control unit (PSCU) mounted on MASCOT (left) [23]; photo of calibration assembly mounted in-vessel by the MASCOT (top-right) [24]; RH system for deployment: boom and MASCOT in JET torus (bottom-right).

which continuously monitored its neutron emission rate during the in-vessel calibration, and activation foils which provided the time integrated neutron yield. The NG and the monitoring detectors were carefully characterized and calibrated in advance at National Physical Laboratory (NPL) [23].

About 76 hours of irradiation over 9 days with the neutron generator positioned at 73 different poloidal and toroidal locations in-vessel were required to calibrate the two main neutron diagnostics: the ^{235}U fission chambers of KN1 (reference diagnostic for time-resolved neutron yield rate measurements) and the KN2 inner activation foils system (main system for integral neutron yield measurements). The calibration factors for DT plasmas were derived from direct measurements of the response functions, with corrections provided by detailed neutronics analyses performed with MCNP Monte Carlo code. In particular, extensive MCNP simulations were performed to determine the KN1 calibration factors for DT plasmas. These calculations were essential to account for the specific calibration setup, including the use of a point source with defined characteristics and the presence of the neutron generator, RH boom and MASCOT, which introduce differences compared to actual plasma operation conditions. First, the responses of the KN1 fission chambers to the NG source positioned on the central ring, alongside the RH system were computed for all experimental configurations. This was done using the MCNP model of the NG and its validated source subroutine from NPL campaigns, along with the MCNP model of the JET device, RH system, and Torus Hall. Next, the same KN1 responses were calculated for an isotropic DT neutron point source with a Gaussian spectrum on the central ring, but without the RH system. Finally, calculations were carried out for a DT plasma scenario to compare the results. This study provides the total correction factors of 1.04 in D1 (Oct 8), 1.10 in D2 (Oct 2) and 1.19 in D3 (Oct 6). More details are in [24].

The calibration campaign was successful and consistent with the 2013 calibration using ^{252}Cf, with some differences attributed to modifications inside and outside the machine, as well as the anisotropy of the NG emission. The total uncertainty on the calibration factors for both KN1 and KN2 was ±6%, well below the requested target accuracy [24].

During the DTE2 campaign, several high-yield shots were measured for a rigorous cross-calibration of the U-^{235} and U^{238} fission chambers of KN1 [25]. These measurements were fundamental for ensuring the accuracy and consistency of neutron yield assessments across different monitors in the various ranges of operations. Furthermore, multiple dosimetry foil measurements from the KN2 activation system showed excellent agreement with the expected results and NPL data, further validating the reliability of the methodology and stability of the systems. During the experimental campaigns, continuous monitoring and cross-calibration checks between the fission chambers and the activation system were performed to ensure consistency in the neutron yield measurements and to maintain with time a high level of accuracy in the derived yields from both diagnostics. More recently, during the DTE3

campaign, further calibration efforts were undertaken. Slight modifications to the calibration factor were implemented due to updates and improvements in the geometry and plasma source models, reflecting the continuous evolution and refinement of the calibration methodology to improve accuracy and reliability to reach the 10% uncertainty value. Fig. 6 shows the optimal correlation and linearity between KN1 and KN2 neutron yield measurements over a wide range of DT operations and consistency with NPL data. A detailed assessment of the uncertainties was also performed demonstrating the fulfilment of the ±10% target [25].

The 14 MeV neutron calibration experience at JET provided valuable outcomes and several lessons were learnt for future calibrations in ITER. The implemented methodology was proved to be successful for the characterization of the 14 MeV neutron generator, calibration of monitoring detectors and in-vessel operation with its power supply units, detectors, and electronics. The careful studies, in-depth analyses, modeling efforts and continuous checks and cross-calibration during plasma operations demonstrated the feasibility to reach and maintain the required measurement accuracy of 10% or even below in DT operations.

However, the size and higher level of complexity of the ITER machine, the wider range of neutron emission to be covered (7 order of magnitude: from 10^{14} to 7.5×10^{20} n/s) and the differences in type and locations of neutron detectors, will require that the procedure validated at JET is modified and adapted to ITER.

One of the major challenges is the achievement of the requested accuracy within the limited time available for the operations. From the JET experience, a proper combination of central ring scans and reference scans was found to be sufficient for calibrating the active neutron yield detectors, while a few carefully selected calibration positions were suitable for the validation of the neutronics model used for the KN2 activation foils system [24]. A proper selection of these in-vessel positions will be particularly crucial in ITER machine, considering its size and limited time for calibration.

The fidelity of the neutronics models, the reliability of the codes, and the accurate knowledge of the detectors response functions proved to be of key importance for the determination of JET calibration factors. This will be more challenging in ITER due to its larger dimensions and increased machine complexity, making the calibration factors derived from radiation transport simulations even more critical. The verification of the accuracy of the neutronics models and reliability of the simulations will be essential to ensure both for absolute calibrated systems and for cross-calibrated diagnostics.

Compared to JET, much more intense NG (10^{9} -10^{10}n/s) will be needed in ITER to meet its calibration needs. It will be heavier, need for active coolant, more complex RH and in-vessel calibration assembly, requiring a thoughtful preparation. A careful characterization is essential, together with the accurate calibration of the active monitoring detectors to monitor its neutron emission rate.

It is recommended that the entire calibration setup, including the neutron generator, monitoring detectors, and all connections, should be tested on-site in real working conditions. Furthermore, a bunker for the deployment of the NG is necessary [24]. This facility will enable the safe operation of neutron sources, the calibration of detectors, and the testing of all calibration equipment to ensure the reliability and accuracy of the procedure.

Moreover, the use of robust and stable techniques, multiple redundancies in detection systems and diagnostics, regular model update and verification, as well as continuous cross-calibration will be necessary to be implemented in order to mitigate the risk.

It should be pointed-out that, based on JET experience, while calibration with Cf-252 combined with MCNP-based energy correction can reduce uncertainties compared with NG, the reliability of such an approach depends on the validation of the neutronics model, in particular for more complex machines where deviations from ideal conditions may arise.

4.2. *Activation of real ITER materials*

ITER material samples were irradiated for the first time in a tokamak D–T plasma environment operating at significant fusion power levels to characterise and validate the codes and data used to predict neutron-induced activation in ITER [26]. A total of 27 materials from various ITER components were exposed to the D-T nuclear environment, including poloidal field coil jackets, toroidal field coil radial closure plate SS316L(N) and SS316L steels, SS316L(N)-IG for vacuum vessel plates, Reduced Activation Ferritic/Martensitic (RAFM) steel EUROFER97, tungsten (W) and CuCrZr from the divertor, SS304 and Alloy 660 from the ITER in wall shield (IWS), Inconel-718, XM-19 for divertor cassette forgings, as well as Al-bronze for the inner vertical target (IVT). The samples were located in a dedicated holder and installed in the Long-Term Irradiation Station (LTIS) near the JET vacuum vessel (see Fig. 7) [27,28]. In this position, the neutron flux in high-performance shots reached 2×10^{13} n/cm^2/s, which is only one order of magnitude lower than expected as ITER First Wall for 500 MW pulse, as discussed in Section 3. During the DTE2 experiment, the samples were exposed to JET plasma over 715 days and more than 3000 shots. In this period, 8.67 $\times$ 10^{20} neutrons were produced by JET operations resulting in a total

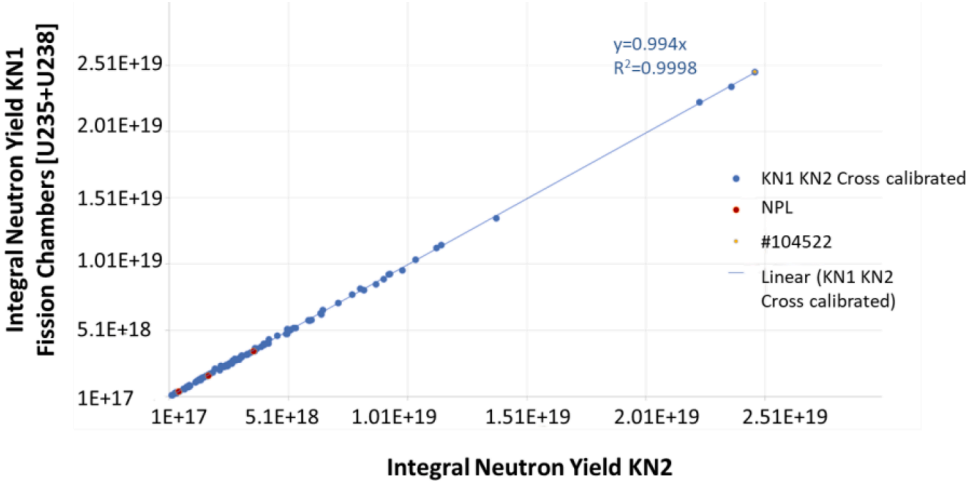

Fig. 6. Correlation of integral neutron yield measurements during DT with KN1 and KN2 in the range 10^{17} n/cm^2 to 2.5 $\times$ 19 n/cm^2 (fusion energy record pulse). NPL data are also shown [25].

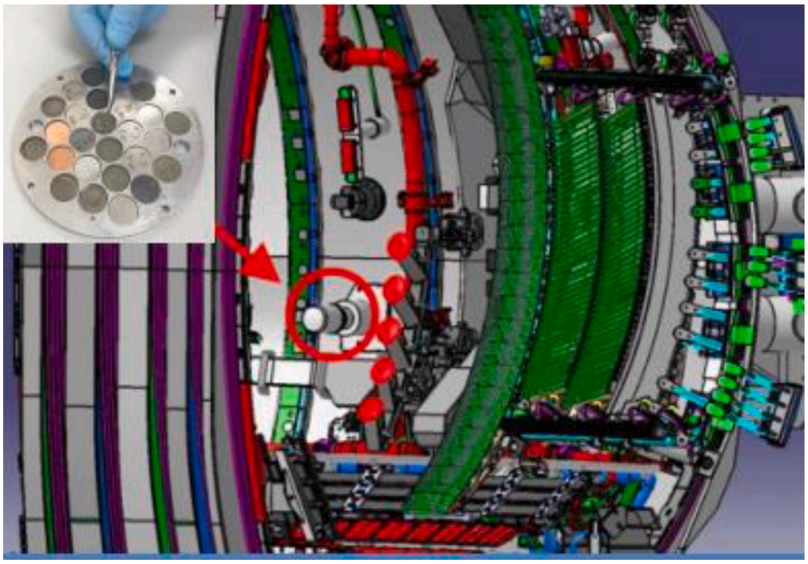

Fig. 7. Sample holder and LTIS location in JET.

neutron fluence in LTIS holder of 5×10^{15} n/cm^2. DD, DT and TT operations were performed during the exposure, but the activation is mainly due to the D-T phase. High-resolution gamma spectrometry techniques were used by five European laboratories (ENEA, IFJ PAN, IPPLM, NCSRD, and UKAEA) to analyse the 68 post-irradiated samples and accurately measure neutron-induced activation levels and identify the radionuclides. Passive neutron diagnostics included 25 dosimetry foil-based activation detectors and two *noVEl neutRon Detector for fusIon* VERDI spectrometers [29]. Moreover, 12 samples for positron annihilation spectroscopy were irradiated.

The gamma spectrometry results were compared with simulations performed using the MCNP6 [30] radiation transport code with FENDL-3.1b [31] and the FISPACT-II [32] inventory code. FISPACT-II calculations used multiple nuclear cross section data libraries to model neutron activation accurately. The highest priority was given to IRDFF-II nuclear data [33], followed by JEFF 3.3 [34] pointwise data, with the remaining reaction channels covered by TENDL-2017 [35] group-wise activation data.

These simulations were conducted with a detailed 3D JET neutronics model of the tokamak that included the LTIS, as well as the specific geometry and chemical composition of the samples, based on certificates from the manufacturers. The irradiation history was defined using the neutron yield rate values derived from the main JET neutron diagnostic systems.

The calculated activities (C) were compared with experimental data (E), providing C/E ratios. The C/E values for different ITER material types are shown in Fig. 8 [26]. In general, with some exceptions, isotopes such as ^{46}Sc, ^{51}Cr, ^{54}Mn, ^{57}Co, ^{59}Fe, ^{95}Nb, and ^{181}Hf showed C/E values close to 1, within 25%. However, significant overestimations were observed for some radionuclides relevant to shutdown dose rate assessments, in particular ^{58}Co (e.g. $C/E \approx 8.6$ in CuCrZ and $C/E \approx 7.3$ in W), ^{60}Co (e.g., $C/E \approx 3.29$ in SS316L(N)), and ^{182}Ta (e.g. $C/E \approx 60$ in CuCrZr, $C/E \approx 17$ in XM-19 and $C/E \approx 13$ in Inconel-718).

While ^{60}Co results were underestimated in EUROFER97, Alloy 660, SS304, W and (e.g. $C/E \approx 0.33$ in EUROFER97), other materials, such as Al-Bronze and SS316L(N)-IG, had C/E values close to 1, within 25%. Some low C/E values were found for ^{65}Zn, whose presence was explained by contamination from brass wire used during the sample cutting with electrical discharge machining (EDM). An unexpected presence of ^{110m}Ag was detected in CuCrZr and Al-bronze [36]. Moreover, ^{182}Ta was found in Alloy 660, SS316L, and SS316L(N). Samples of CuCrZr, and tungsten monoblocks showed more significant deviations compared to other samples.

In summary, good agreement between calculations and measurements was observed, particularly for nuclides generated by fast neutrons, although some discrepancies were evidenced. The observed discrepancies, especially in cobalt isotopes and CuCrZr and tungsten samples, may arise from uncertainties in material impurities concentration and MCNP modelling geometry and contamination. Nuclear data uncertainties play a minor role. Similar trends were observed in previous DD experiments [28]. Inaccuracies in elemental composition in material certificates likely contribute to deviations, and independent analysis

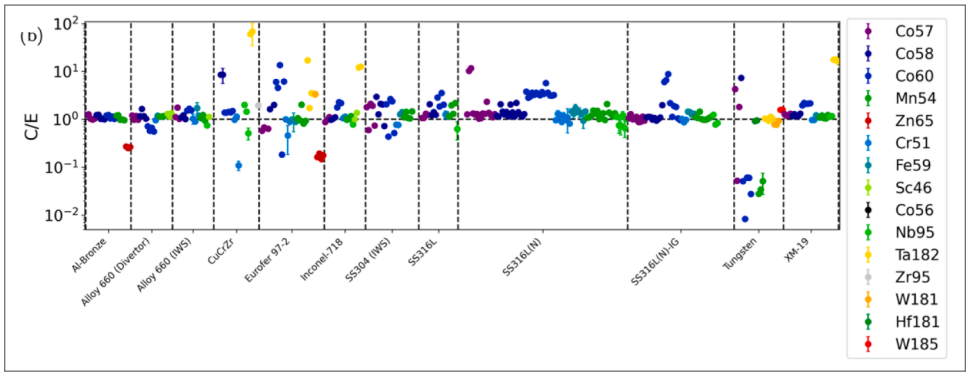

Fig. 8. C/E values of the activity of the various isotopes per ITER material. Reproduced from [26].

using advanced analytical techniques such as inductively coupled plasma mass spectrometry (ICP-MS) are ongoing to improve accuracy.

The study provided unique experience in characterizing and studying neutron activation in ITER materials within a tokamak environment under significant nuclear conditions. The results have demonstrated the reliability of the MCNP6 and FISPACT-II codes, along with modern nuclear data, in accurate prediction of neutron-induced activation, with conservative results generally expected for nuclides relevant to maintenance operations. The use of High-Purity Germanium (HPGe) with Compton Suppression Systems (CSS) improved measurement sensitivity and the signal-to-background ratio compared with standard HPGe measurement. Manufacturing and cutting techniques were identified as potential sources of contamination, emphasizing the need for precise material composition evaluations. A new holder with polished samples was installed during the DTE3 campaign, and post-analysis is currently ongoing. Furthermore, samples of W have been exposed in the irradiation-end during some DTE3 shots to study short-term activation. More sensitive radiometric and mass-based measurement techniques will be employed to extend the characterization of long-lived nuclides, in particular those relevant for waste management and decommissioning.

4.3. Neutron induced-damage studies

The DT campaigns also offered a unique opportunity to study material damage under 14 MeV neutrons in a harsh environment. In particular, limited data are currently available on the radiation resistance of functional materials under fusion-relevant conditions. Understanding the effects of fast neutron irradiation in tokamak operating conditions is crucial for ITER and future machines. Although the maximum level of damage during the DTE2 and DTE3 campaigns was on the order of 10^{-5} dpa, even at this low level, degradation of the physical properties of functional materials may already occur and affect the functioning of the systems.

Dedicated experiments were conducted to assess the degradation of the optical and dielectric properties of functional materials due to fast neutron and gamma irradiation during the TT and DT campaigns at JET [5,6].

The study includes Post-Irradiation Examination (PIE) of selected insulators irradiated close to the JET vessel and real-time in-situ measurements of optical fiber transmission.

4.3.1. Assembly for PIE of optical and electrical behaviour of insulators

Several types of insulators typically used in diagnostics and heating systems of fusion machines were selected and characterized in the CIEMAT and NCSRD laboratories in terms of optical, electrical, structural and chemical properties before exposure at JET. A proper holder with passive samples was installed adjacent to the samples for activation study in LTIS position in September 2020 and irradiated until the end of JET operations in 2023. Selected materials included alumina (quite different purities), sapphire, Spinel, CaF2, a-SiO2, BaF2, YAG, AlN Si3N4 and diamond [37]. The configuration of the holder and it location is shown in Fig. 9.

The samples have been retrieved from JET on June 2024 and the PIE examination is expected to be performed in CIEMAT and NCSRD laboratories in 2025. The optical spectrum of transmission or reflection (for non-transparent samples) will be measured using a commercial photometer for the UV–VIS-NIR range and a Fourier Transform spectrometer in the IR range. These same samples were previously characterized before being irradiated. The comparison between both spectra will allow for the evaluation of damage caused by irradiation. Electronic defects will be studies through Photo-Induced thermally Stimulated Current (PITSC) method.

It should be noted that surface contamination and erosion/corrosion phenomena could also affect optical transmission and/or reflection. A relevant and measurable effect due to erosion is not expected because the samples are located outside the vacuum chamber. Only some minor deposition of sputtered material from the sample holder on the optical samples could introduce a measurable background signal in the optical characterization. This effect will be analyzed anyway; however, it is not expected to have a significant impact on the optical characterization of the irradiated material.

4.3.2. In-situ real-time optical transmission of optical fiber measurements during DT

In-situ measurements of optical fibre evolution with accumulating DT pulses and recovery phases were performed during TT and DTE2 campaign. Hermetically sealed metal-coated fused silica optical fibers were exposed to neutron and gamma irradiation at JET in LTIS. The experimental configuration includes a double lamp as light source (halogen and Deuterium lamps), a multiplexer to switch between different fibers (including the reference one, not irradiated, to provide baseline), and the spectrometer to measure the optical transmission spectrum of the fiber. The fibers are installed so that they enter the

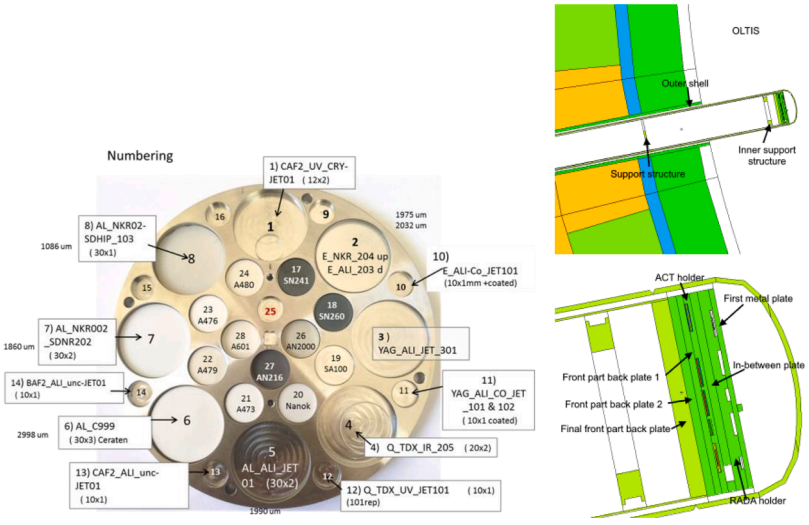

Fig. 9. (left) Sample holder for radiation damage study with all the functional material samples loaded and code numbering for the various materials; (right) horizontal section of LTIS model in JET octant 7 (top): details of the assembly of activation samples (ACT) and radiation damage (RADA) holders in LTIS MCNP model (bottom).

active port of the torus in the LTIS position and return to the control room. Light is sent through the fibers, and the transmitted spectrum is collected over time (Fig. 10).

Degradation of optical transmission under DT irradiation is evident from Fig. 11; a clear decrease in optical transmission across wavelengths (200–1200 nm) with increasing neutron flux (up to ~5×10^{15} cm^2), due to radiation-induced defects is clearly seen. Specific peaks in the absorption spectrum correspond to different defects in silica, as identified from literature [38,39]. These defects, caused by neutron irradiation, include oxygen-deficient centers (ODC), self-trapped holes (STH), and non-bridging oxygen hole centers (NBOHC). The evolution of these peaks varies with the total dose due to different formation energies and annealing mechanisms. The results, even if preliminary, provide insights into neutron-induced defects and their dependence from cumulated fluence. A detailed study is ongoing to decouple neutron and gamma radiation effects and preliminary evaluation evidenced some differences. Comprehensive pulse analysis is also in progress to evaluate the potential recovery of the transmission between pulses.

4.4. Test of neutron and tritium detectors for ITER TBM

Accurate and reliable measurement of the tritium production rate in breeding blankets (BBs) is essential for proving the self-sufficiency of tritium fuel supply and ensuring proper tritium inventory control in future fusion reactors. Test Blanket Modules (TBMs) in ITER will offer the first experimental validation of predictions related to tritium production and recovery in BBs. Developing and testing nuclear instrumentation to measure neutron and gamma flux, as well as tritium production in TBMs, is a major challenge, as the instrumentation must operate in a harsh environment with temperatures up to 650 °C, high magnetic field and neutron and gamma flux intensity up to 2×10^{14} n/cm^2/s and 4.5×10^{13} γ/cm^2/s, respectively in 500 MW pulses [40]. DT operation at JET provides a unique opportunity to test some detectors under development for TBMs, both active and passive systems, in a real fusion environment.

As for active systems, two Single Crystal Diamond detectors (SCDs), one of the two equipped with a ^{6}LiF layer to detect thermal neutrons, were located in the periscope port of octant 3 to test their response in hostile conditions (i.e., temperature up to 320 °C, magnetic field of about 3 T, neutron flux of 5×10^{12} n/cm^2/s). After some malfunctioning observed during DTE2, they have been partially tested in-place, thus excluding any faults in the measurement chain. Due to the limit imposed by dose rate, they could not be dismounted for further testing or repair in home-lab and were not operated during the subsequent DTE3 campaign. The future retrieval will allow to perform inspections and tests to identify the cause of the failure, i.e., if related to electric connections or the hostile environment (temperature, vibrations, etc.).

A third SCD was employed for a benchmark experiment to validate the calculation of the tritium production rate in TBMs in a real fusion environment across DTE2 and DTE3. It was carried out in a mock-up of the Helium Cooled Pebble Bed (HCPB) TBM, earlier used at the 14 MeV Frascati Neutron Generator (FNG) [41]. The mock-up was located close to the main horizontal port of Octant 8 (Fig. 12) and the SCD detector, covered with a thin LiF layer, inserted in the second (of four) diagnostic channel to measure in real-time the tritium production rate during DT operations (Fig. 13) through neutron detection. Such a detector was earlier calibrated at the standard thermal neutron source of the ENEA metrology institute (INMRI), to determine the calibration coefficient which correlates thermal neutron flux and tritium reaction rate. Tritium production measurements across some DTE2 pulses were then compared against MCNP6 calculations based on the full (360°) model of JET in which the HCPB mock-up and SCD detector were implemented [42]. The magnitude of neutron flux level on the SCD detector, in high-performance DT operations, was up to 4.5×10^{11} n/cm^2/s.

The key outcomes from measurements during DTE2 pulses are summarized as follow: a) the system is capable of monitoring the neutron emission across the temporal pulse evolution in low performance (as long as the neutron emission rate of JET does not exceed 10^{15} n/s), in agreement with the JET neutron monitor (KN1) based on fission chambers; b) the tritium production rate measured (E) is 1.40×10^{-12} tritons per source neutron. A comparison against MCNP simulation (C) provides a ratio C/E of 0.77 [42]. This conservative prediction is consistent with previous results obtained at FNG under 14-MeV neutron irradiation. Above 10^{15} n/s, pile-up events became predominant and an upgrade of the measuring chain was done to speed up the measuring chain. The amplifier was replaced with a faster one and during DTE3 the system proved to work properly up to 3×10^{17} n/s (i.e. neutron flux 3×10^{10} n/cm^2/s at the detector location). Such a value is close to the maximum data transfer rate through USB between the detection system and the computer, as evident in Fig. 14, bottom plot, where intermittent signal dropouts occur during a high-performance pulse. As the amplifier was substituted, a new calibration of the detection system is necessary to determine the tritium production rate.

Several lessons were learnt so far on detector design and operation and some extrapolation to ITER TBM have been drawn [42].

The main consideration and key design modifications needed to adapt the diamond system for ITER TBMs based on JET experience are summarised below:

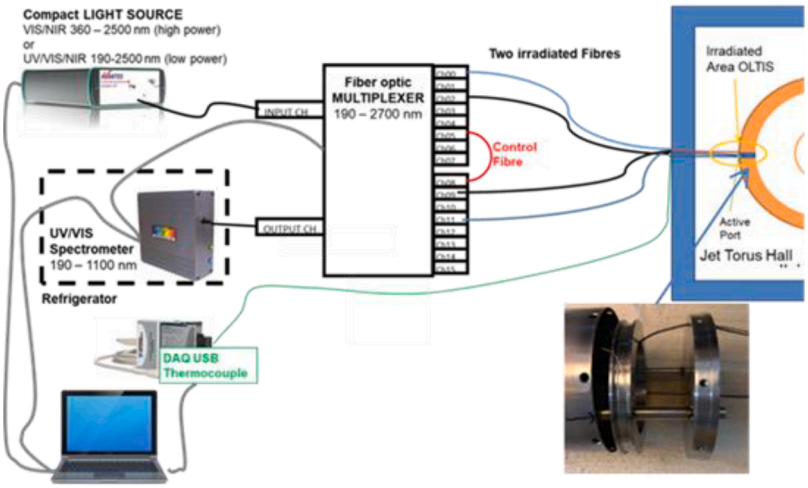

Fig. 10. Layout of the experimental assembly for the real-time study of degradation of optical fiber transmission. The insert shows the photo of the optical fiber in the spool behind the RADA sample holder in LTIS.

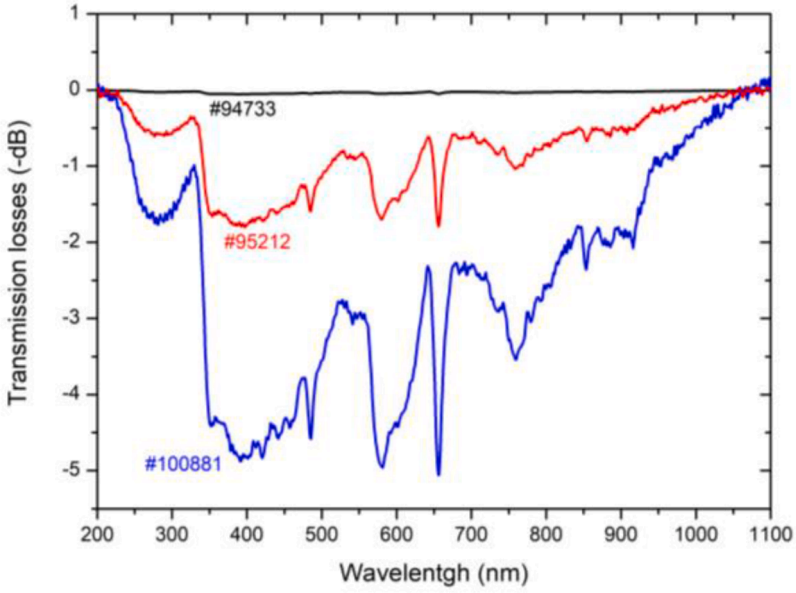

Fig. 11. Transmission losses vs. wavelength for total neutron fluence of about ~2 × 10^{13} cm^2 (pulse #95212, 14/09/2019) and ~5 × 10^{15} cm^2(pulse #100881, 26/08/2022). 0 refers to the not-irradiated reference level (after the pulse #94733, 13/08/2019).

Fig. 12. Photo of the HCPB TBM mock-up installed close to the front collimator of the beamline in Octant 8. The dimensions of the HCPB TBM mock-up are 30 × 29 × 31 cm^3. The stainless steel box is filled with beryllium and it contains two steel double cassettes filled with Li_2CO_3 powder [38].

— The neutron flux in ITER TBMs is expected to be 100–1000 times higher than in the TBM mock-up at JET, corresponding to an increase of approximately two orders of magnitude. This significantly impacts detector performance, requiring modifications to efficiency and signal processing to avoid excessive count rates and signal pile-up.
— To adapt to the higher flux, the detection efficiency must be reduced. This can be achieved by reducing the thickness of the LiF converting layer or using natural Li instead of 95% enriched ^{6}Li to lower the cps-to-neutron-rate ratio and prevent detector saturation.
— The measuring system at JET showed issues to process detection events with high plasma neutron emission rate, causing pulse pile-up. For ITER, the charge preamplifier, identified as the bottleneck, must be upgraded to handle the increased event rate efficiently. Moreover, connecting the digitizer to the computer via optical fiber would improve the maximum data transfer rate by almost 2.7 times compared to USB, enhancing real-time data acquisition and processing capabilities.
— ITER conditions require detectors and cables that can withstand elevated temperatures. Mineral-insulated cables with alumina insulation are necessary, but at 300 °C, their leakage current increases by four orders of magnitude, which must be minimized to keep the measurement accuracy.
— Due to limited accessibility for maintenance in ITER, reliable electrical connections resistant to vibrations and accidental impacts are crucial. Issues such as poor pin-to-cable connections observed in JET must be addressed to ensure long-term system stability.

As for passive detection system, several efforts have been also performed to develop and test at JET a Neutron Activation System (NAS) for neutron flux spectra measurements in ITER TBM. Stacks of foils have been selected based on the reactions and measurability of the product nuclides for exposure in KN2 irradiation ends. The measured activities are used to calculate the neutron spectrum via unfolding techniques using the SPECTRA-UF suite [43]. Measurements have been performed in KN2 3 Upper and 6 Upper across the DD, TT and DT campaigns. Out of the four shots requested, two shots were successfully delivered to KN2 6 Upper during DTE2, one containing indium only and the other containing a stack of various material foils (Cr, Cu^{89}/Sn^{11}, Nb, Al^{90}/Ce^{10}) [44]. The foils were returned via the pneumatic transfer line to a 190% relative efficiency HPGe detector, and data was recorded in list-mode format. The measurement set-up is shown in Fig. 15. Short-lived nuclides were difficult to measure due to a delay between the end of irradiation and acquisition. The analysis identified ^{24}Na, ^{27}Mg, ^{51}Cr, ^{51}Ti, ^{52}V, ^{90m}Y, ^{92m}Nb, ^{94m}Nb and ^{116m}In in the activated foil stack, and ^{24}Na, ^{114m}In and ^{115m}In in the activated indium foil. Some of the identified nuclides are considered not usable for neutron spectrum unfolding due to either their potentially unknown origin (i.e. ^{24}Na) or undetermined solution. First attempts at neutron spectrum unfolding were not successful. Some improvements were attained with efficiency re-calibration using an updated MCNP model of the detector and measurement layout, in particular for In-foil. Further analyses and optimisation of SPECTRA-UF unfolding techniques are ongoing to accurately reproduce the spectrum.

4.5. Neutronics benchmark experiments

In high performance tokamaks the radiation field during and at the

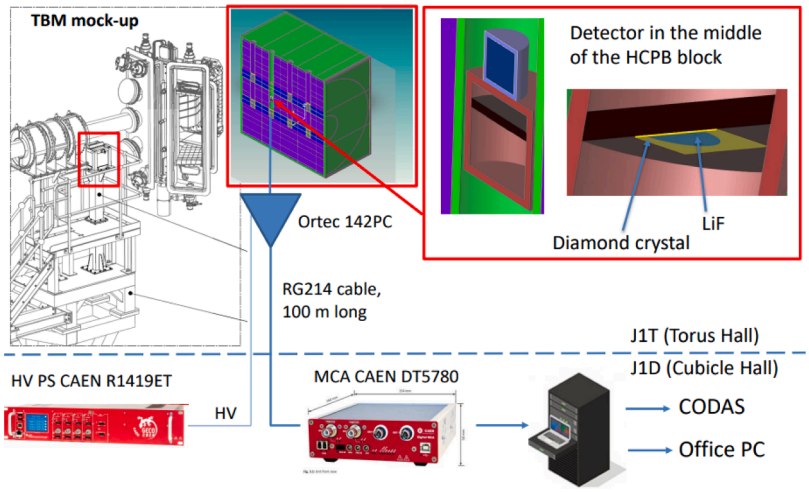

Fig. 13. Layout of the experimental assembly of the SCD detection system installed at JET inside a diagnostic channel of the HCPB TBM mock-up. 3D view of octant 8 with HCPB TBM mock-up in red (left); middle-section of the MCNP model of the HCPB mock-up (middle); diamond detector MCNP model (top-right). The scheme of electronics used for DTE2 measurements is also shown (bottom) [38].

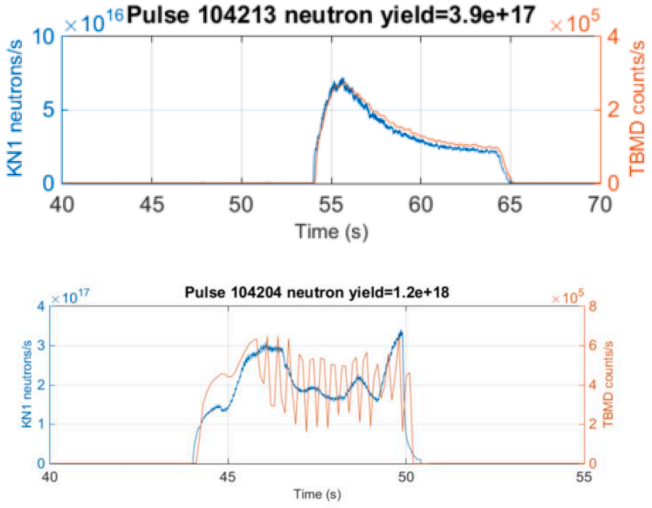

Fig. 14. Temporal profile of counts/s measured by the diamond detector (in orange) compared to the neutron rate from KN1 neutron monitor based on fission chambers (in blue), during two pulses of DTE3 below (top) and above 3 $\times$ 10^{17} n/s (bottom).

end of operations is extremely complex. The calculation of the neutron flux and the derived nuclear quantities in ITER and future reactors is very challenging, in particular far from the plasma, due to large and complex geometries, presence of narrow penetrations in thick shields and many different materials involved. Under neutron irradiation, the tokamak's components undergo activation, causing a complex gamma field with large spatial and temporal variation even when the machine is not operating. In particular, the prediction of the shutdown dose rate (SDDR) caused by neutron activation is a critical safety task in fusion reactors for planning of intervention and maintenance operations, ensuring that dose limits remain within safe limits. The overall accuracy of the computational tools employed for nuclear analyses, during and at the end of operations, cannot be easily evaluated mainly because of the lack of experimental data for their validation in real fusion tokamak environment. ITER-oriented experiments have been performed at JET to assess the prediction of neutron streaming calculations through the JET biological shield and the shutdown dose rates aimed at validating the state-of-art codes and nuclear data used in ITER nuclear analyses [45,46].

Several measurements and code benchmarking have been conducted in the last decade during the DD campaigns before tritium operations for both shutdown dose rate [45–51] and neutron streaming [46,52–55],] experiments. The gained experience and detailed pre-analyses allowed to optimize the detectors assembly, calibration protocols and experimental techniques, refine the modelling, improve the computation tools to reduce the uncertainties of the benchmarks in DT operations.

4.5.1. *Neutron streaming experiment*

Dedicated measurements were performed during TT, DTE2 and DTE3 in the years 2021–2023. The cumulated neutron fluence was measured using proper assemblies of thermo-luminescent detectors (TLDs) and activation foils (AF) [22,23]. The detectors were placed in 21 positions close to the machine and in South-West labyrinth and South-East chimney spanning over 8 order of magnitude variation in neutron fluence from the plasma up to 40 m away from it. The arrangement for the MCP-N and MCP-P TLDs inside moderators was optimized to reduce the interference between detectors and the shadowing effect based on experience in DD [52]. Accurate calibrations were performed in neutron and gamma fields [56,57].

The calculations are performed using MCNP6.2 [58] with ADVANTG [59] and TRIPOLI-4© [60] using plasma neutron sources generated by D-D, T-T and D-T reactions and a three-dimensional 360° neutronics model that includes JET components, torus hall (TH), basement and detailed detectors assemblies representation (Fig. 17) [53,54].

Preliminary results of TT benchmark experiment have been recently published [61]. The TLDs and AFs for TT have been installed at the end of 2020. All TLDs and AFs in moderators were retrieved and replaced with detectors for DT at the end of July 2021 (before the start of DTE2), except for TLDs in the most shielded positions, where the expected cumulated neutron fluence was close to background level. The total neutron yield during exposure was 8.50 $\times$ 10^{18}, of which 59.3% was generated by T-T reactions, 40.2% from D-T due to deuterium residual in plasma chamber and the rest from D-D. JSI, UKAEA and ORNL teams carried-out the simulations using MCNP6 for radiation transport and ADVANTG for weight windows generation using the same JET MCNP model and tallies. The 360° MCNP model was converted into TRIPOLI-4© representation [62] and the calculations performed by CEA. The preliminary results of the TT experiment are shown in Fig. 18. Except for the most shielded position B8 (at the exit of SW labyrinth), the differences in MCNP results from the various parties are within ±7%. The TRIPOLI-4© results are consistent with MCNP results within ±10%. The comparison of the combined neutron fluence results of the

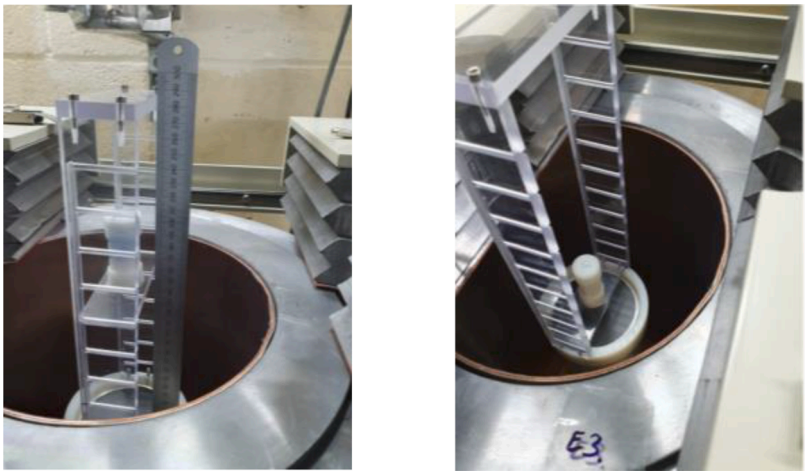

Fig. 15. Measurement setup of the foils activated during the DTE2 campaign in KN2 6U: Multiple foil stack irradiated in shot #99959 (left) and In foil irradiated in shot #99976 [40].

simulations in TLDs positions from ORNL, UKAEA and JSI and preliminary TLDs experimental data from IFJ shows the ratio of the calculation over experiment (C/E) that varies in the range ~0.4 in A1 (on the platform of KT1 spectrometer) to ~2.9 in B5 (on the chimney floor, between ducts). An increase of the overestimation of the calculations with the distance from the machine is observed, showing a similar trend to previous results. However, except for A1, in which the C/E is slightly worse than in latest DD streaming experiment in 2019 [46,53,54], an improvement between calculations and experiment has been achieved.

The calculation of the reaction rates in AF were performed by ORNL and JSI and compared with AF measurements from NCSRD [61]. For $^{59}Co(n,\gamma)^{60}Co$ and $^{181}Ta(n,\gamma)^{182}Ta$ reactions, the calculation slightly underestimate the measurements in position A1 and overestimate the experiment in the other positions. The largest overestimation, up to a factor 9, is found for $^{109}Ag(n,\gamma)$ ^{110m}Ag in position A4 (at the top of inner SW labyrinth), maybe due to modelling inaccuracy affecting thermal neutron component in the region of resonance of this reaction. However, it should be noted that the results are significantly improved compared to previous DD campaign [54]. Advancements are achieved thanks to improved calibration of the detectors, enhanced accuracy in JET neutron diagnostics calibration (used for normalization) and improvements in model and computational tools. Completion of analyses of TT and DT measurements are ongoing, corroborated by response function studies of TLDs to improve the accuracy for DT applications. In parallel, model upgrades, especially in the South East area, are performed, to improve the representation of the walls and penetrations. Model conversion into OpenMC code [63] is also ongoing to validate also this open-source Monte Carlo code through JET neutron streaming measurements.

4.5.2. *Shutdown dose rate benchmark experiment*

On-line shutdown dose rate measurements were performed by ENEA with dosimetry system based on ionization chambers (IC) installed on special shelves on the side port of octant 1 close to the Radial Neutron Camera and in one more shielded position in octant 2 on the top of ITER like Antenna (ILA), behind poloidal field coil (Fig. 19) [45]. AF assemblies from NCSRD, containing sets of silver, cobalt, iron, yttrium, rhodium, titanium, zinc, and nickel foils in aluminum boxes, were placed near the ICs to measure the neutron fluence. For DTE3, AF aluminum boxes with and without flexible B_4C sheets from CERN on both sides, were also positioned in octants 1 and 2, as well as in A2 (on the top of outer lab in west wall, see Fig. 16), to test its neutron shielding performance. The flexible B_4C shield is used also in the SEE project to test its performance in protection of electronics (see Section 4.7).

Three low-activation detectors were used for shutdown dose rate measurements, two of these gamma dosimeters are 140 mm diameter air-vented spherical ionization chambers. A third smaller IC with 44 mm diameter for high dose rate measurements has been located in octant 1 close to the bigger one. Each IC is connected to its electrometer located

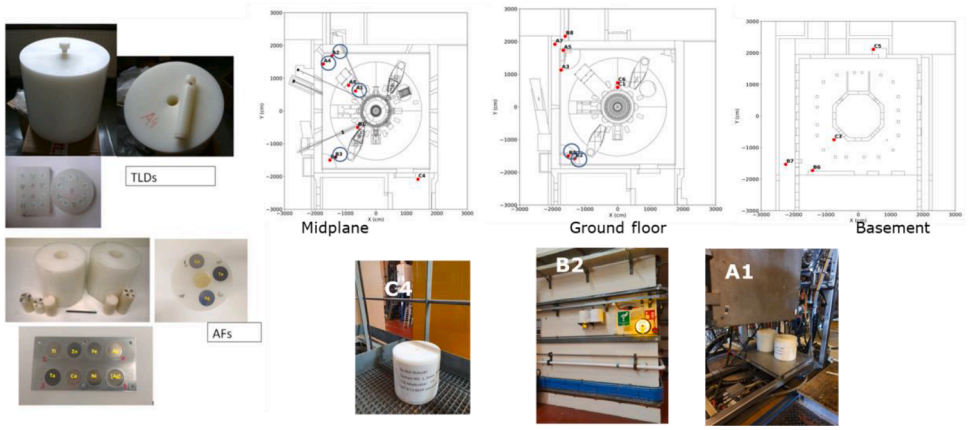

Fig. 16. Photos of TLDs (top-left) from IFJ and AFs (bottom-left) from NCSRD assemblies. Top right: positions of TLDs for DT experiments at the mid-plane, ground floor and in the basement; activation foils in polyethylene moderator are located in circled positions (i.e. A1, A2, A4, B2, B3 and B5). Bottom right: photos of the assemblies located in position C4, B2 and A1.

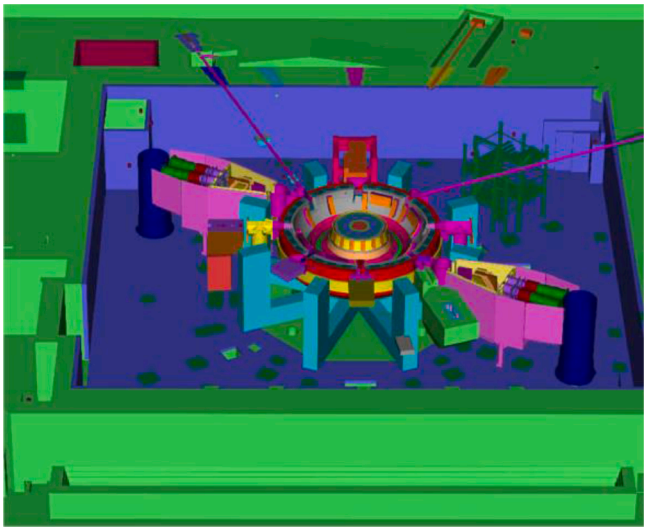

Fig. 17. JET 360° MCNP model [57].

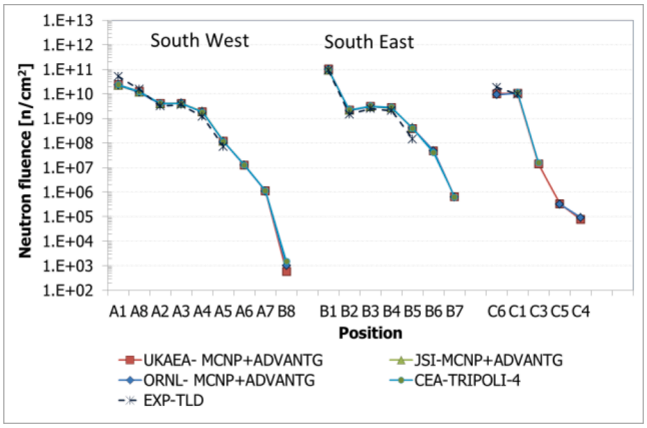

Fig. 18. Neutron fluence in TLDs positions: calculated neutron fluence combining 59.3% TT and 40.2% DT and 0.05% DD from UKAEA, JSI, ORNL and CEA and preliminary TLDs experimental data from IFJ during TT campaign.

in J1D cubicles through high-quality and low noise tri-axial cables. The software for remote control and acquisition was settled to manage the acquisition and data sharing with CODAS [49,64]. Prior tests, measurements and simulations confirmed that activation of the IC housing and air has only a minor impact on the total dose beyond short cooling times [45,48].

The system is operating since 2016 [47,49] and it is still on-operation during the decommissioning. It has proved to be robust, reliable, with a few interruptions occurred along these years. The results of the measurements during the first phase of TT campaign and DTE2 have been recently published [64,65].

Fig. 20 shows the measurements in the last phases of DTE2 and DTE3. The upper plots show the neutron yield of each pulse from KN1 diagnostic and on the same time-axis, the air kerma rate (in μGy/h) measured by the ion chambers in the bottom panels. The plotted data are obtained by converting raw signals into air kerma rate (by applying calibration factors) and such data is also corrected for influence quantities (e.g., air conditions, oxygen concentration in the torus hall) [65].

The dose rate measured in octant 1 is higher than in octant 2, because the latter detector is shielded by ILA structure, while the octant 1 midport is almost empty. The gamma decay in octant 2 is faster than in octant 1 as predicted by pre-analysis as well, as dominated by the activation of copper in the front poloidal field coil. The shutdown dose rate level varies in the range from ~30 μSv/h to ~20 mSv/h in octant 1 and from ~3μSv/h to ~5 mSv/h in octant 2. Some differences are observed in exponential decay of the two chambers in octant 1 for DTE2. At dose rates lower than 50 μGy/h, the behavior is due to the low sensitivity of the smaller chamber. At higher doses the different temporal trend is due to the different position on the shelve. Due to a technical problem the measurements in octant 2 were interrupted on 7 December 2021 and only data in octant 1 are available during the DTE2 shutdown. The peaks of air-kerma rate are in correspondence of neutron emission during JET pulses. Along those periods the signal does not represent a measurement of dose as it exceeds the upper limit of the measuring range.

During the tritium clean-up campaign following DTE3 the dose rate remains high with inter-pulse level ~500 μSv/h in octant 1 and 20 μSv/h in octant 2. At the end of 2023 the dose rate level decreases to ~400 μSv/h in octant 1 and 15 μSv/h in octant 2. It should be noted that the range of dose rate levels measured during JET DT operations is highly relevant for ITER, where design constraints for hands-on maintenance specify limits of 100 μSv/h in the port interspace 12 days after shutdown, and 10 μSv/h in the port cell 1 day after shutdown. Thus, such measurements represent a unique database to validate codes in ITER relevant conditions. To eliminate the influence of short-lived air vented activation, important at short cooling times, only data collected at least two hours after shutdown are considered for benchmarking.

The results of these measurements are used for the experimental validation of Rigorous Two-Steps (R2S) [66–70] and Direct 1- Step (D1S) [71–78] tools for ITER shutdown dose rate predictions by comparing numerical prediction against SDDR measurements at JET. In R2S approach, neutron and decay gamma transport calculations are performed separately, whereas in D1S, a single simulation integrates both neutron and decay gamma transport simultaneously.

The calculations with the various codes were performed using 45° MCNP models of octant 1 and octant 2 (Fig. 21) with reflecting surfaces, including detailed representations of detectors assemblies and surrounding components on the basis of CAD and drawings and with the materials chemical compositions with impurities from available documentation. The JET neutron irradiation history used to calculate the activation at the time of the experiment is based on neutron rates measured by JET KN1 monitor. Only D-T component was considered because of the contribution from D-D and T-T reactions is negligible during DT campaigns.

Preliminary results of shutdown dose rate calculations for DTE2 with MCNP-based SDR tools are reported here. The analyses refer to the following tools:

- AdD1S (Advanced D1S dynamic) [74,75]: improved version of D1S code based on MCNP5 [21] developed by ENEA in 2011 with mesh tally capability [71,73]. FISPACT [32] is used to derive the time correction factors. Special libraries are used.
- D1SUNED [76,77]: developed by UNED is currently the most advanced D1S tool, reference for ITER nuclear analyses. It is based on MCNP6 [58]. Time correction factors are calculated analytically. Special libraries are used.
- N1S [78] is a hybrid tool recently developed by UKAEA. It requires a single radiation transport calculation, as D1S, while removing the need for pre-calculations to determine dominant nuclides and time correction factors.
- MCR2S [67,68]: R2S code developed by UKAEA and based on MCNP6 [58] and FISPACT II [32] using the cell-under-voxel (CuV) method.
- R2SUNED [69]: R2S tool based on MCNP6 [58] for radiation transport and ACAB [79] for neutron activation developed by UNED. It uses the cell-under-voxel (CuV) method.
- ORNLR2S [80]: R2S tool developed by ORNL that implements the multi-step consistent adjoint driven importance sampling (MS-CADIS) technique to determine optimal variance reduction parameters

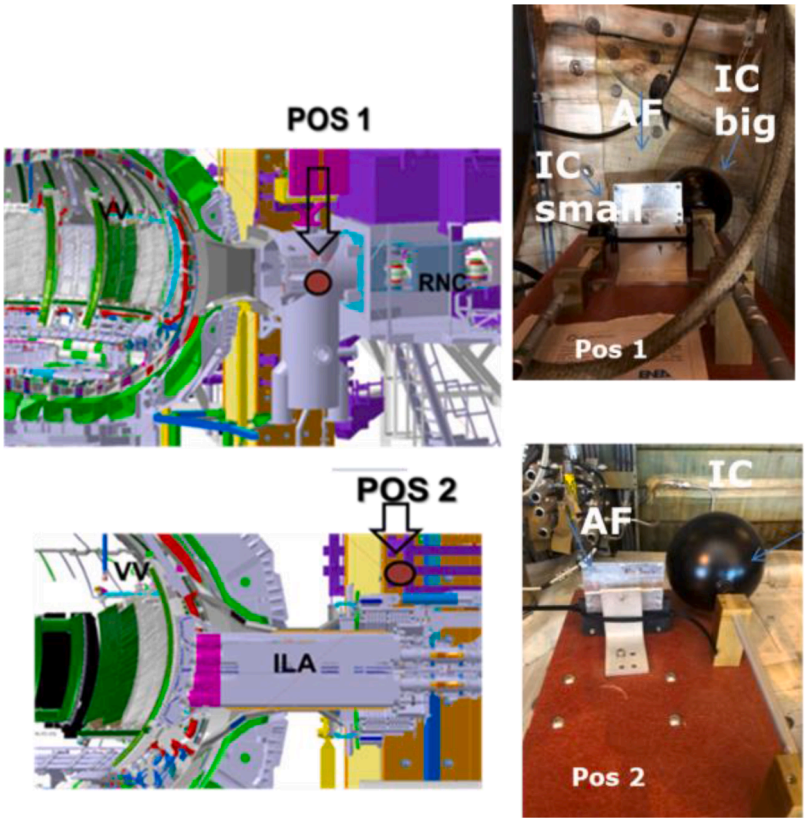

Fig. 19. Positions of Shutdown Dose Rate detectors in Octants 1 (top-left) and 2 (bottom-left). Photo of the ICs and AF assembly located in octant 1 (top-right) and octant 2 (bottom-right) [41].

for the final quantity of interest-the SDDR. ORIGEN [81] is used for activation analysis.

Concerning nuclear data libraries, reference ITER FENDL3.1d [30] and mclib84 were mainly used for neutron and photon transport, respectively. The special libraries used in D1S codes by UNED and ENEA were based on FENDL3.1c.

The temporal evolution of the shutdown dose rate in the big IC in octant 1 at the DTE2 shutdown is shown in Fig. 22. The results of the calculations with the various tools and IC measurements are plotted. In general all codes show similar results (within ±20%) and the same trend, with good agreement with experimental results at short (within one day) and overestimation at longer cooling times. The best results are obtained with N1S code that overestimates the measurements within +20%, while the larger overestimation is found with codes up to +40%. The observed trend is maybe caused by overestimation of ^{58}Co contribution by Inconel components, dominating the shutdown dose rate at these cooling times.

With respect to the previous 2019 shutdown dose rate benchmark after DD campaign [80], the agreement between calculations and measurements is generally improved with all the computational tools employed thanks to model and code upgrades, enhanced accuracy in JET neutron diagnostics calibration and operational history representation.

In octant 2, there is a noticeable range of variation and differences among the approaches, as shown in the Fig. 23 (last shot on 6 November 2021). Among the single-run tools (i.e., Advanced D1S, D1SUNED, and N1S), N1S showed the minor underestimation, with all tools generally providing under-prediction for the measured dose rate throughout the cooling period (from −30% up to −60% at 2 days of cooling time). The underestimation is maybe due to modelling inaccuracy in representing penetration and components, leading to an overestimation of the shielding effect compared to actual conditions.

The higher results obtained with R2S codes at short cooling time, though they are closer to the experimental data, are caused by calculation error due to group-wise energy resolution which induces uncorrected predictions in R2S approach [82]. Indeed, past UNED study evidenced that the discrepancies between R2S and D1S codes in octant 2 at short cooling time are not caused by mesh sizes or some missing activation reactions in D1S codes but due to the energy discretization in R2S codes. This study demonstrated, in particular, that the energy discretization in some resonance regions on ^{63}Cu(n,γ)^{64}Cu, if resonance shielding corrections are not applied, causes an overestimation of the R2S results. As the half-life of ^{64}Cu is 12.7 hours this effect is important for short cooling times (up to 2 days). For other reactions the calculation mismatch due to group-wise energy resolution is less critical. Implementation of point-wise R2S approach overcomes such limitation.

Similar findings have been observed in other phases of the DTE2 campaign, while analyses of DTE3 experiments are ongoing. Recently, simulations with D1S and R2S implemented through OpenMC and TRIPOLI-4© have started. In parallel, a neutron error propagation scheme is being implemented for R2S codes. Dedicated publications will follow.

4.5.3. *Main outcomes for nuclear analyses from JET experience*

The studies conducted so-far demonstrated the reliability of MCNP-based tools when modern nuclear data libraries and accurate modeling (geometry, materials, and machine evolution) are used in nuclear analyses of complex tokamaks. The benchmarks have also identified certain limitations and artifacts within computational tools, driving the development of new features and updates. A precise knowledge of material impurities, operational conditions, and machine configuration changes is essential. Additionally, the JET experience has supported advancements in experimental measurements techniques,

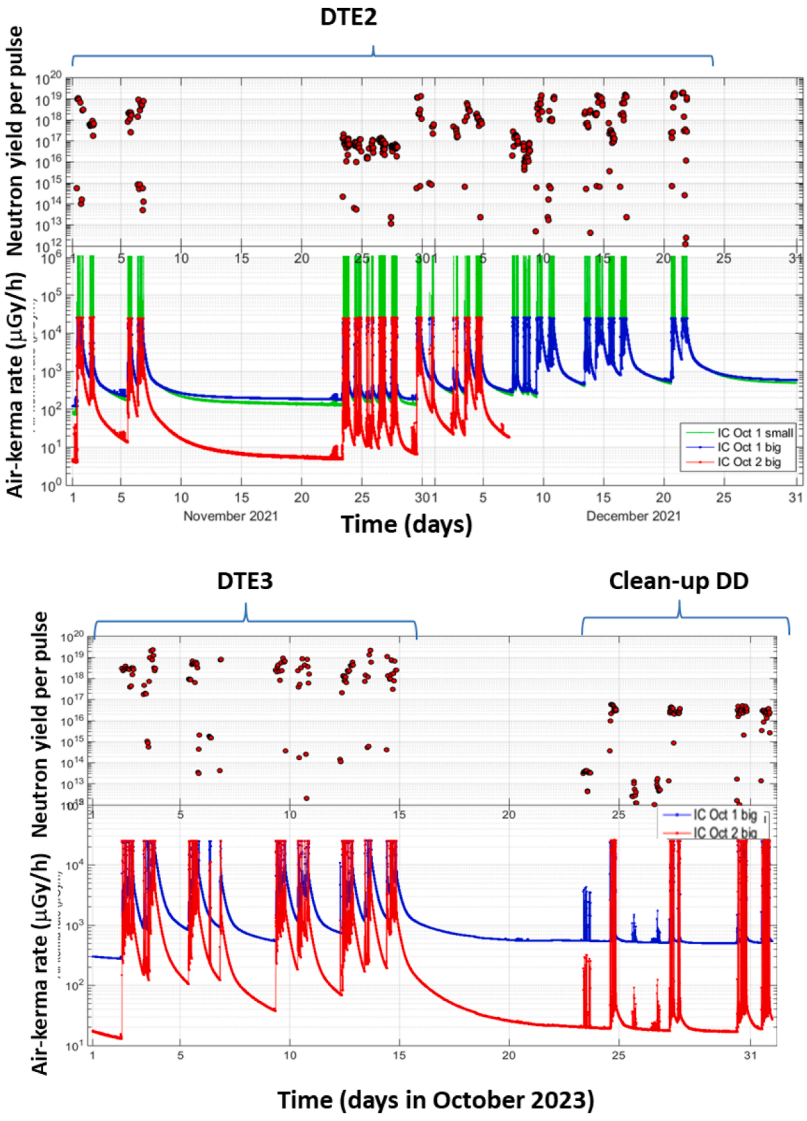

Fig. 20. Neutron yield per pulse (top) and air kerma rate measurements with ICs (bottom) during (a) DTE2 in November and December 2021, (b) last phase of DTE3 and clean-up in October 2023. Small IC was switched-off in 2023, for repurposing its electronics.

which may prove valuable for ITER and other tokamaks.

The primary recommendations to improve the accuracy in nuclear analyses are as follows:

- **Model uncertainty reduction**: ensure detailed representations of geometry and materials, particularly focusing on impurity contents.
- **Continuous update of neutronics models**: keep models aligned with current machine/component evolution.
- **Enhanced detail in geometry and materials**: use CAD for geometry and certified data for materials.
- **Accurate radiation source simulation**: Simulate radiation sources with high fidelity.
- **Materials chemical composition knowledge**: improve understanding of material impurities by performing independent chemical analysis.
- **Neutron yield and irradiation history**: simulate neutron emission rates with minimal uncertainties.
- **Comprehensive irradiation history representation**: define temporal discretisation to accurately simulate both short-lived and long-lived nuclides.
- **Code development**: improve codes to mitigate artefacts (e.g. related to spatial and energy discretization in R2S).
- **Expand and update nuclear data**: regularly update nuclear data libraries.
- **Global Variance Reduction techniques**: implement variance reduction techniques to improve simulation accuracy.

These steps are crucial for advancing simulation accuracy and reliability, supporting both present and future nuclear analyses.

4.6. *Water activation experiment*

During DT plasma operations in fusion reactors, the water coolant undergoes activation due to neutron irradiation, leading mainly ^{16}N and ^{17}N radionuclides. The nuclide ^{16}N has a half-life of 7.13 s and emits gamma rays at 6.129 MeV (67%) and 7.115 MeV (5%). ^{17}N, with a half-life of 4.14 s, primarily emits neutrons, which, when transported, could activate components beyond the primary cooling circuit.

Due to high energy threshold (~10.5 MeV for ^{16}O(n,p)^{16}N reaction and ~9 MeV for ^{17}O(n,p)^{17}N), the activation of water is much higher in ITER and future fusion reactors compared to fission reactors [83]. Water activation, in particular gamma rays from ^{16}N decay, can induce nuclear loads in sensitive tokamak and plant components, e.g. nuclear heat in superconducting magnets, absorbed doses in polymer-based

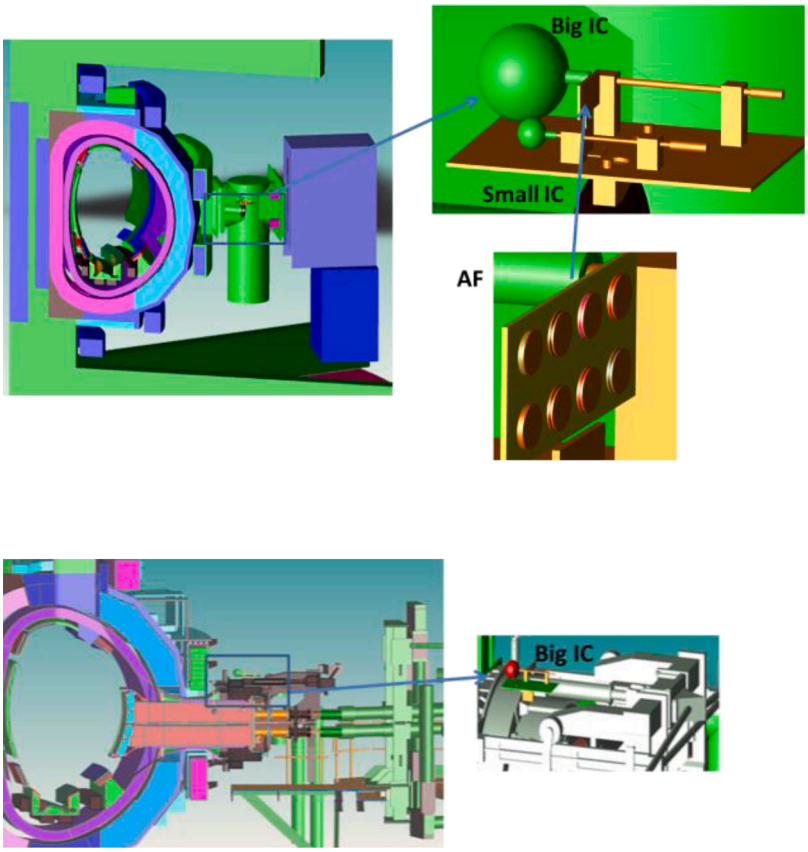

Fig. 21. Octant 1 (top) and Octant 2 (bottom) MCNP model with SDR experimental assembly. Details of IC and AF are shown.

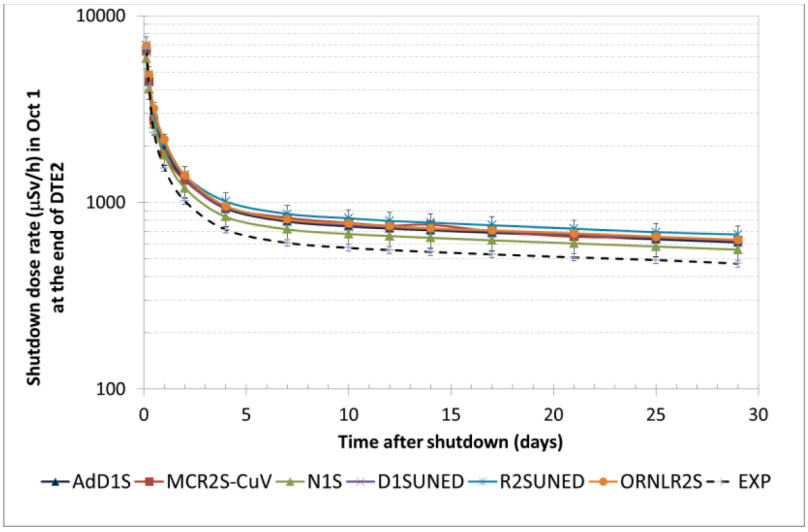

Fig. 22. Shutdown dose rate calculated with D1S and R2S codes and experimental data from big IC in OCT1 during DTE2 shutdown versus cooling time from the last pulse of 21 December 2021.

components such as valves, or high dose rates in electronics [84]. The radiation loads due to activated water are calculated using complex models and multi-physics methodologies considering exposure, activation, flow velocity and decay for individual water volumes in all different loops [85–87]. The activated water is one of the main radiological concerns in ITER, but the uncertainties in the calculation are large, mainly due to modelling and nuclear data and experimental benchmarking is crucial but experimental data is extremely limited with 14 MeV neutrons.

Previous experiments oriented to fusion environments were performed with DT neutron generators at FNS [88] and FNG [89–91], while a new water cooling loop, i.e. KATANA, has been recently installed at the fission research reactor (TRIGA) of JSI [92].

In this context, JET represents a unique opportunity to investigate the phenomena with a real tokamak water cooling loop exposed to high-energy neutrons from D-T reactions. This allow for the validation of the complete methodology used to assess water activation in ITER and the implementation of diagnostics system based on water-activation.

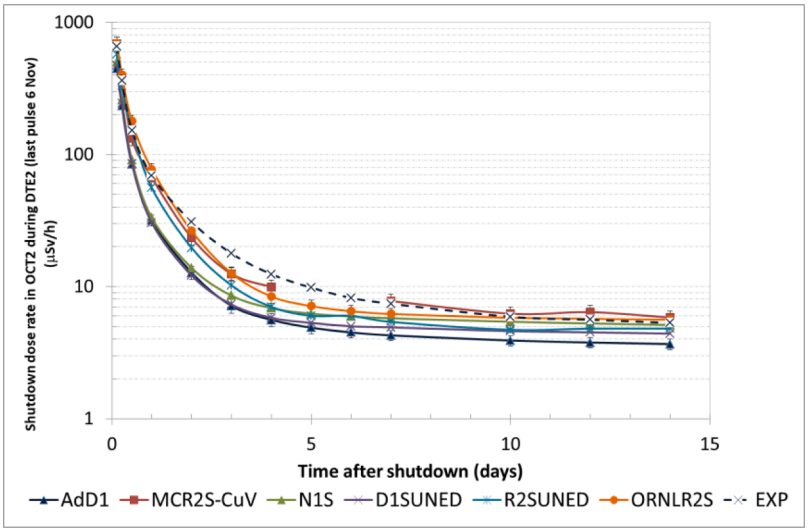

Fig. 23. Shutdown dose rate calculated with D1S and R2S codes and experimental data from IC in OCT2 during off-operational period of DTE2 versus cooling time from the last pulse of 6 November 2021.

In 2017, a feasibility study was performed for installing a water activation measurement at JET for DTE2. The findings of this assessment confirmed its feasibility [93]. However, the activities were put on hold in 2018, due to insufficient resources available from the JET operator to support its preparation.

Given its critical relevance for ITER and DEMO, the experiment was re-proposed as one of the main technological goal of the DTE3 campaign.

Two scintillators, already available at JET and previously tested under laboratory conditions [93] have been used as gamma spectrometers. They are based on 3 × 3 inches crystals of sodium iodide doped with thallium (NaI (Tl)) and bismuth germanate ($Bi_4Ge_3O_{12}$), referred in the following as NaI and BGO. The gamma spectrometers, with shields and collimators, have been installed in 2023 in the basement of octant 4 close to the horizontal outlet pipe collecting the water from the Neutral Beam Injector (NBI) duct scraper and Rotary High-Vacuum Valve (RHVV) cooling loops. Fig. 24 shows the CAD of JET octant 4 with the cooling loop of interest and the location in the basement of the WACT system. Photos of the pipe forest in the basement of octant 4 and of the WACT assembly and detectors are in Fig. 25. Detectors were also calibrated in-situ with the WACT assembly using various gamma sources.

Proper custom software, i.e. PHOENIX, was developed by ENEA to trigger, perform real-time data acquisition, and interface with CODAS to measure the high energy gamma energy from ^{16}N decay correlated with JET plasma operations.

The installation of the WACT system faced numerous challenges and deviations from the original plan due to various technical issues, water flooding in the basement, procurement delays, and complexities in original setup. These problems required quick solutions constrained by tight schedule, resulting in significant deviations from the optimised design, that originally foresaw more massive shields and the use of an ionization chamber to complement the experiment with dose rate measurements.

However, despite the problems occurred, significant and unique measurements have been performed during DD, DTE3 and tritium clean-up campaign, with over 1500 shots covering five orders of magnitude range of neutron yield and pulse length up to 60 s [94,95]

Fig. 26 shows the measurements with BGO spectrometer for the DD shot #104074 (total neutron yield 3.09 × 10^{16} n), a few days before the start of the DTE3 campaign. The temporal evolution of the neutron yield rate measurement with KN1 is also shown. Gamma energy spectra during and at the end of plasma operations are compared. Delayed gamma started appearing after 11 s and peaked approximately 16 s after the start of the plasma shot. The observed counts in BGO during operations are due to prompt gamma. Clear and well-resolved high-energy peaks from water activation at 6 and 7 MeV were visible, and the

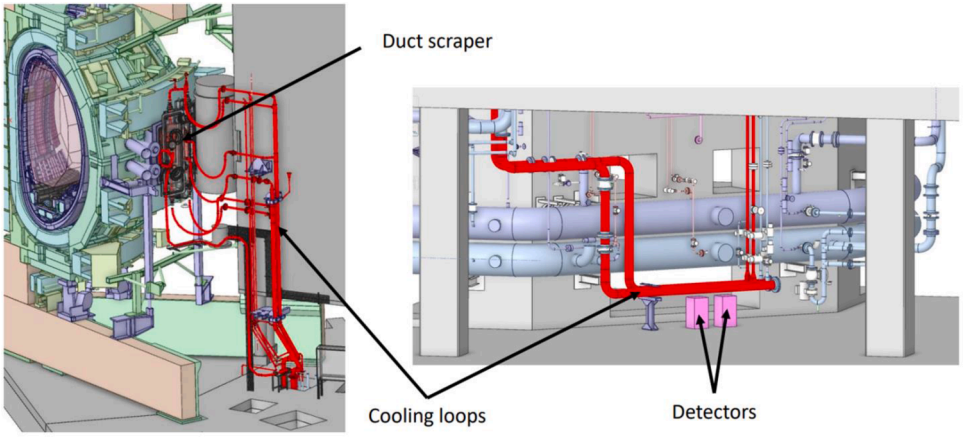

Fig. 24. CAD of the JET octant 4 Torus Hall (left) and Basement (right) with NBI duct Scraper cooling pipes in red. A simplified representation of the detectors' assembly is shown in pink.

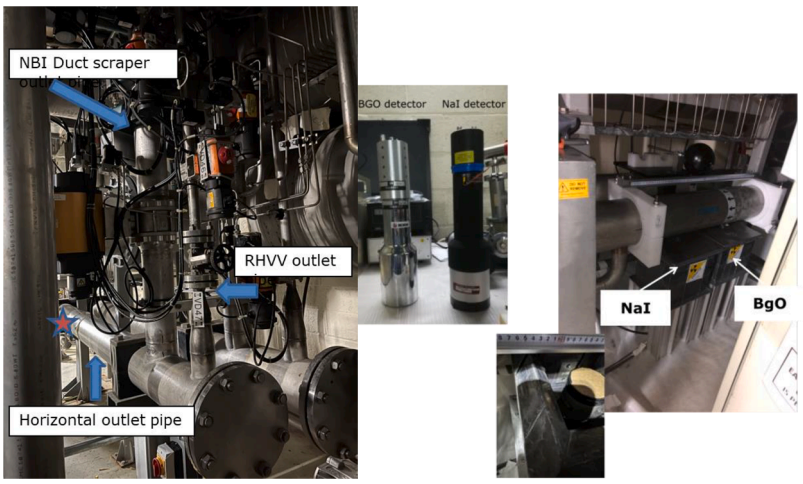

Fig. 25. Vertical outlet pipes from NBI duct scraper and RHVV and horizontal big outlet pipe in octant 4 basement; the location of WACT system is shown with a star (left). NaI and BGO scintillation detectors used for the experiment (middle). Photo of the WACT assembly with NaI and BGO located in lead shield and collimators below the horizontal big pipe (right); the insert shows the NaI with permanent gamma source inside.

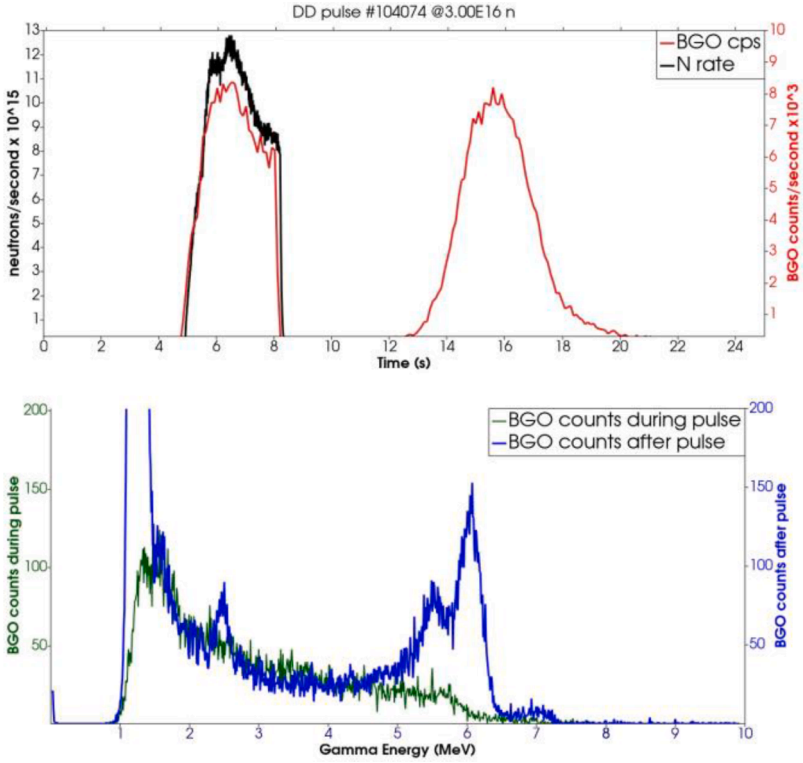

Fig. 26. Total neutron yield rate (n/s) and gamma count rate (counts/s) in BGO versus time (s) from the start of the DD pulse #104,074 on 24 August 2023 (top); gamma energy spectra (counts vs. energy) in BGO during plasma shot and at the end of shot (bottom). Two shield plates with small collimators were placed on the BGO detector.

maximum count rate was 8×10^3 cps due to activation induced by about 3×10^{14} DT neutrons from triton-burnup. In general the BGO measurements during DD campaign showed clear delayed gamma signal from ~7 s and peaks at ~11–12 s after the start of neutron production with duration of ~10–15 s.

Fig. 27 shows the measurement taken with BGO during the JET DT shot #104175 on 24thAugust 2023 (DT neutron yield 2.63×10^{18} n). The DT yield observed here was more than four orders of magnitude higher than during DD shots. The delayed signal appeared at 14 s after start of shot and rapidly increased to a level exceeding 10^5 cps. Following prompt-gamma measurements a breakdown lasting few seconds occurred. Subsequently, two delayed peaks with long tails were observed. Clear water activation peaks were observed in the gamma spectra, representing **the first water activation measurements in a tokamak under DT plasma operations.** It should be noted that the delayed gamma phase observed under DT conditions is considerably longer than during DD shots, revealing a second peak in the temporal behaviour. This might be attributed to ^{16}N gamma from the second cooling RHVV loop, where water activation is lower and delayed due to reduced water velocity compared to the other cooling loop. This second peak is not visible in DD pulses because the activation of the water flowing in RHVV is too low to provide a detectable signal. Gamma

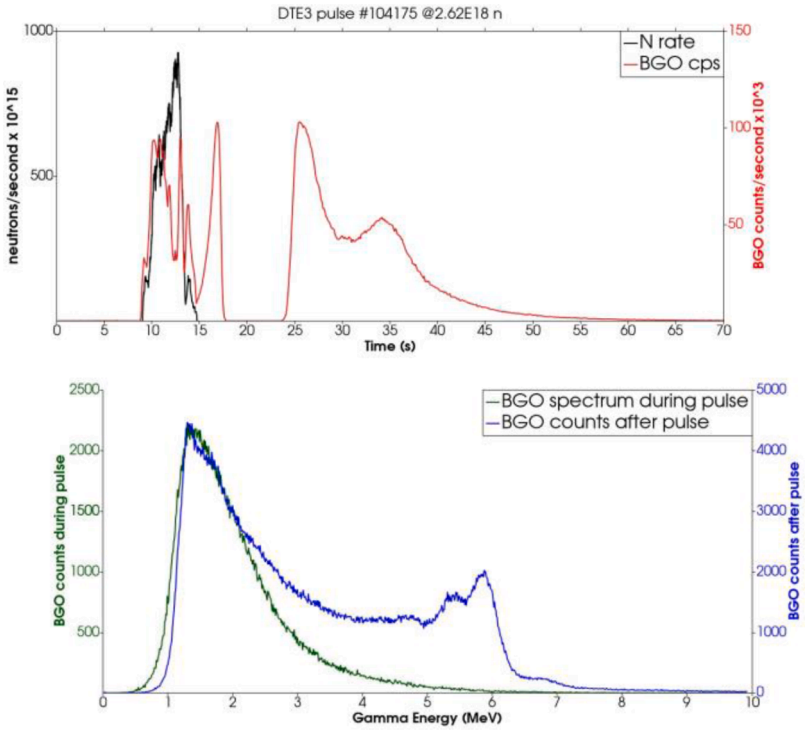

Fig. 27. Total neutron yield rate (n/s) and gamma counts in BGO versus time (s) from the start of the DTE3 pulse #104,175 on 5 September 2023 (top); gamma energy spectra in BGO during plasma shot and at the end of shot (bottom). Four lead shielding plates with medium and small collimators were placed on BGO.

produced by neutron activation of the materials might also contribute.

Similar trends were observed for other shots. Very high count rates in high performance shots $>10^5$ cps leading to black-outs, pileup and slow data rate transfer but the ^{16}N high gamma energy peaks are generally visible in raw data of BGO and can be isolated following proper elaboration. The NaI spectrometer (not shown) exhibited more severe pile-ups obscuring the high energy signal. Manual acquisition using CAEN COMPASS software with pile-up rejection feature and optical link was conducted in parallel for some shots and the analyses are ongoing.

The measurements continued even during clean-up and DD phase until the end of JET operations. Long pulse (up to 60 s) DD sessions were performed between 24 November and 12 December 2023. Fig. 28 shows the measurements performed during the JET longest pulse, #105,750 lasting about 60 s. This scenario is particularly representative of ITER and DEMO conditions where long pulses are expected, and the water activation loads are significant during plasma operation.

BGO signal shows similar trend as the total neutron yield rate but following a more complex shape and long-lasting compared to shorter pulse measurements. During the long operations the BGO signal includes the prompt-gamma as well as delayed gamma from activated materials and water. This does not occur during very short pulses because the transit time from the NBI duct to the basement is longer than the shot duration.

Dedicated spectral analyses across various temporal and energy ranges are currently ongoing to carefully analyse the observed results and improve the understanding of such complex phenomena and plasma physics correlation.

The produced data will be used for validating various tools employed in water activation assessment. The experimental data collected will be simulated using several computational Fluid Activation Tools, including ActiFlow and GammaFlow [89,96]; DEMO Computational Fluid Activation Tool [97,98]; FLUNED [99,100] and Radioactive Species Transport Model (RSTM) [101,102].

Furthermore, the present experience is highly relevant for the development of a dedicated neutron diagnostics system based on water-activation for tokamak applications.

4.7. *Neutron-induced single event effects on electronics*

The interaction of neutrons with electronic components can cause significant issues, including damage to devices, signal corruption, and data or program errors in circuits like memories, FPGAs,

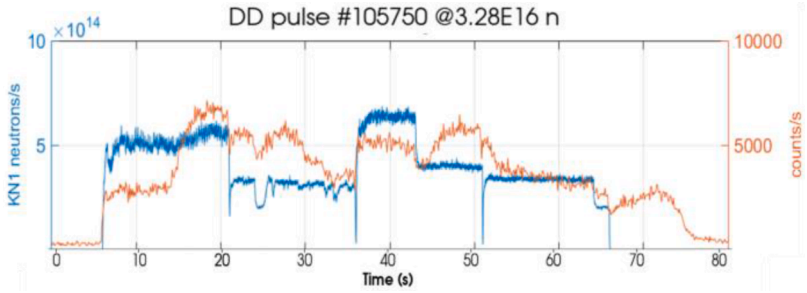

Fig. 28. Total neutron yield rate (n/s) and gamma count rate (counts/s) in BGO versus time (s) from the start of the record long (59.97 s) DD pulse #105,750 on 12 December 2023. No collimators were placed on BGO.

microcontrollers and microprocessors. These effects can occur gradually over time or instantaneously from a single neutron interaction, referred to as a Single Event Effect (SEE). The SEEs induced by neutrons on electronics are one of the most difficult problems facing high performance tokamaks and accelerators with a significant impact on the reliability [103,104,106]. Unique systematic study of the Single Event Upsets (SEUs) induced by neutrons on electronics was conducted during DTE3 at JET to validate the single event rate prediction models in tokamak under DT operations [105]. SEUs are SEEs causing bit-flips in memories. The experimental setup for SEU tests was installed in the JET basement in position B6 behind the south wall (close to the TLDs of neutron streaming experiment reported in Section 4.5) as shown in Fig. 29. In this position the average neutron flux in DT operations is about 3×10^5 n/cm^2/s (same level as expected in the ITER port cells). The experimental setup includes two test benches composed of CMOS SRAM (static random-access memory) components widely used in modern Commercial off-the shelf (COTS) electronics. One of them, operated by the University of Marseille, hereafter referred to as "RTSER test bench", integrates 384 bulk 65 nm SRAM circuits from STMicroelectronics (with a total of 3.2 Gbit). It was previously tested at WEST under neutrons from DD plasma operations with energy ranging from thermal up to 2.45 MeV [103–105]. The other one, operated by CERN, hereafter referred to as "CERN test bench", is made up of two bulk 40 nm SRAM circuits from Integrated Silicon Solution Inc. (ISSI): one of them is covered with 5 mm of B_4C flexible shielding (containing 80% of B_4C) and the other is bare. This 40 nm SRAM was previously studied under neutrons with energies ranging from thermal to 20 MeV neutrons [107, 108]. Both test-benches were previously characterized at other facilities, with response functions and models developed and benchmarked in different radiation fields. A DIAMON (Direction-Aware Isotropic and Active Monitoring) neutron spectrometer from RAYLAB was installed at the location of the RTSER and CERN test benches for real-time neutron spectra measurements. The systems are monitored and controlled remotely. Close to the experimental setup, passive systems, i.e. activation foils and Passive Neutron Spectrometry (PNS) system, were also located to collect further information on cumulated neutron fluence and spectra.

The accumulation of SEUs versus cumulated neutron fluence for RTSER and CERN test benches are shown in Fig. 30 and Fig. 31, respectively. In the RTSER test bench, SEUs were either Single-bit upsets (SBUs) causing one single bit-flip, or multiple-cells upsets (MCUs) causing several bit-flips (up to 9). In the CERN test bench, all SEUs were SBUs (no MCU). The RTSER showed a bit-flip rate of 493 bit-flips/hour/Gbit, while in the CERN test bench, the bit-flip rate was significantly higher at 2342 bit-flips/hour/Gbit. The reliability degradation factor (RDF) compared to natural environment is very high in both systems (9.34×10^6 for RTSER and 9.60×10^6 for CERN), highlighting the severity of the effect. In Fig. 31, the comparison of the results obtained with the CERN test bench with and without B_4C shielding shows a clear reduction in bit-flips by a factor of 4.3 with B_4C shielding. However, this improvement is not enough to recover the reliability, suggesting that further enhancements in shielding design are necessary in this environment, due to the presence of high energy neutrons.

Comparison of the JET DTE3 results with bit-flip predictions, based on models developed and already validated through experiments at WEST under DD plasma neutrons and at other neutron facilities, shows excellent agreement. The calculation-to-experiment (C/E) ratios are 0.87 for RTSER and 1.07 for CERN, validating the methods and models used for predicting neutron-induced bit flips, even under DT operations [105].

This activity is part of a broader study of the sensitivity of modern electronics to neutron-induced SEEs, aimed at providing essential data for designing shielded areas in tokamaks and in high-energy accelerators. The goal is to ensure a neutron environment that allows the operation of COTS electronics without the need for special qualification or the use of radiation-hardened components.

The JET experiment and the subsequent studies will have a significant impact on the design and safety of ITER and high-performance tokamaks for the definition of shielding requirements of electronics devices in radiation protected areas, for the design of COTS-based custom radiation tolerant electronic systems, and for the demonstration of the reliability of the COTS electronic systems [105]. In particular, these present and future works will help to more accurately (quantitatively) determine whether an area is radiation-safe or not for electronics operation, and which shielding may be required to achieve an acceptable reliability. In an area that is not (or not enough) radiation shielded for operation of critical electronics with the required reliability, they will provide the SEE sensitivity data needed to design COTS-based custom radiation tolerant electronic systems (e.g. redundant systems) compliant with reliability requirements.

These works, which primarily target tokamaks and particle accelerators, are also potentially interesting for nuclear facilities such as nuclear fission power plants, neutron test facilities, nuclear medical facilities (because radiotherapy environment may include photoneutrons), etc.

5. Conclusions

Unique scientific achievements have been gained so far from technological exploitation of JET DT campaigns relevant for ITER and future fusion reactors, providing the opportunity to:

- implement a successful method for 14 MeV calibration of neutron diagnostics;
- improve the knowledge on the effects of neutron irradiation on damage of functional materials, material activation, neutron streaming, shutdown dose rate, single-event effects on electronics, tritium production, etc.;
- develop and improve nuclear experimental techniques: gamma and neutron spectroscopy, monitoring and dosimetry; tritium measurements; optical and dielectric characterization;

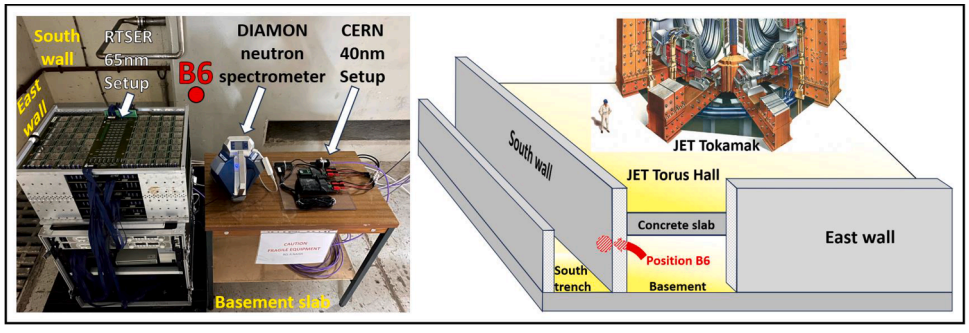

Fig. 29. Schematic drawing of the SEU test-bench position (right) and photo of SEU test-benches and DIAMON spectrometer in B6 position (left).

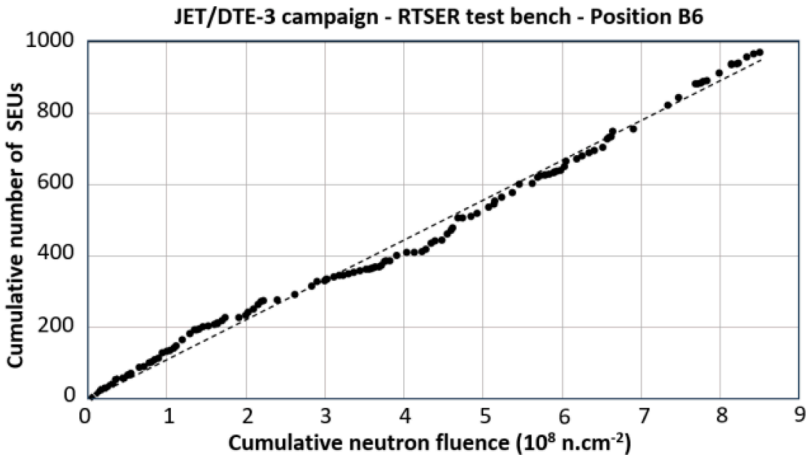

Fig. 30. Cumulative SEUs in RTSER versus cumulative neutron fluence during DTE3 campaign at JET.

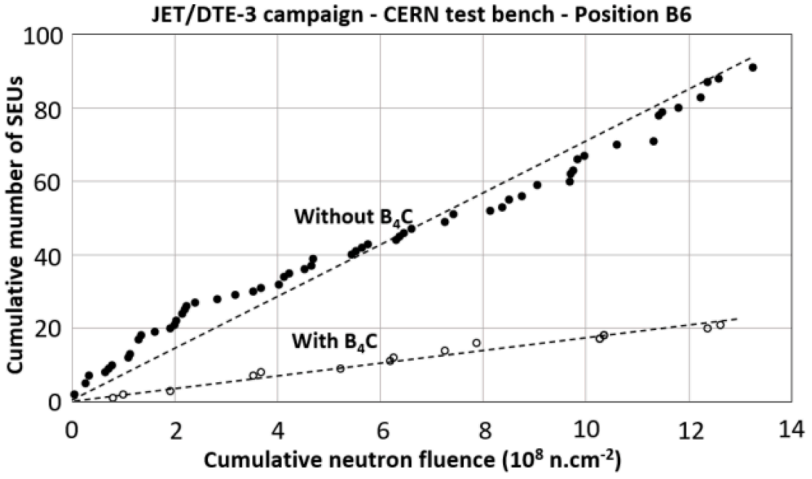

Fig. 31. Cumulative SEUs on CERN test bench, bare (black circles) and covered with B_4C (open circles), versus cumulative neutron fluence during DTE3 campaign at JET.

— develop, optimize and validate nuclear computational tools for radiation transport, activation (materials and water), shutdown dose rates and the coupling with plasma physics and operations;
— demonstrate the reliability of the codes used for ITER nuclear analysis through experimental benchmarking of Monte Carlo-based codes for neutron transport, activation and shutdown dose rate assessment;
— identify critical issues affecting reliability: calibration, neutronics models and nuclear data, materials chemical compositions and impurities, contamination, plasma scenarios and machine evolution; codes bugs and artefacts;
— produce huge database and collected irradiated samples to be used for many further future studies and validation.

The outcomes, experience, and methodologies developed in JET DT operations are becoming even more relevant nowadays, especially in the context of ITER updated re-baseline plan with two DT phases (called DT-1 and DT-2), in accelerating the preparation for its nuclear phase and minimizing risks and uncertainties. The implementation of robust and reliable methodologies and techniques based on JET lessons learnt is important to support the safety demonstrations required for nuclear licensing prior to second DT-2 on ITER. Conducting similar experiments in ITER during the first ITER phases might be extremely relevant in preparation for DT-2 licensing and operations. Through the acquired JET experience, dedicated neutronic experiments in ITER prior and during DT-1 can be valuable to support the safety case for DT-2 across key areas, including activation, damage, radiation streaming, shutdown dose rates, water activation, shielding, activated corrosion products, etc.

JET decommissioning started in 2024 and is expected to take over 10 year: valuable lessons can continue to be learned. International collaboration would benefit the entire community by addressing the challenges and providing further unique insights for the decommissioning of ITER and future power plants.

Declaration of competing interest

The authors declare that they have no known competing financial interests or personal relationships that could have appeared to influence the work reported in this paper.

Acknowledgments

This work has been carried out within the framework of the EUROfusion Consortium, funded by the European Union via the Euratom Research and Training Programme *(Grant Agreement No* 101052200 — *EUROfusion). Views and opinions expressed are however those of the author(s) only and do not necessarily reflect those of the European Union or the European Commission. Neither the European Union nor the European Commission can be held responsible for them.*

Data availability

The authors do not have permission to share data.

References

[1] A. Kappatou et al., Overview of the third JET deuterium-tritium campaign, submitted to Plasma, Phys. Control. Fusion.
[2] C. Maggi, et al., Overview of T and D–T results in JET with ITER-like wall, Nucl. Fusion 64 (11) (2024) 112012.
[3] F. Rimini, et al., 40 years of JET operations: a unique contribution to fusion science, submitted to Plasma, Phys. Control. Fusion.
[4] E. Joffrin, et al., Overview of the EUROfusion tokamak exploitation programme in support of ITER and DEMO, Nucl. Fusion 64 (11) (2024) 112019.
[5] P. Batistoni, et al., Technological exploitation of Deuterium–Tritium operations at JET in support of ITER design, operation and safety, Fusion Eng. Des. 109–111 (2016) 278–285.
[6] X. Litaudon, U. Fantz, R. Villari, et al., EUROfusion contributions to ITER nuclear operation, Nucl. Fusion 64 (11) (2024) 112006.
[7] P. Barabaschi, in: The ITER Project: moving forward to an updated baseline, 33rd Symposium on Fusion Technology, Dublin, Ireland, 2024, 22-27 September.
[8] J.E.T. Team, Fusion energy production from a deuterium-tritium plasma in the JET tokamak, Nucl. Fusion 32 (1992) 187.
[9] M.D. Williams, D-T operation on TFTR, Fusion Eng. Des. 36 (1) (1997) 135–142.
[10] M. Keilhacker, A. Gibson, C. Gormezano, et al., Nucl. Fusion 39 (1999) 209.
[11] J. Jacquinot, V.P. Bhatnagar, J.G. Cordey, et al., Nucl. Fusion 39 (1999) 235.
[12] D. Stork, Yu. Baranov, P. Belo, et al., Nucl. Fusion 45 (2005) S181.
[13] P. Andrew, et al., Tritium retention and clean-up in JET, Fus. Eng. Des 47 (1999) 233–245.
[14] G.F. Mattews et al., JET ITER-like wall—overview and experimental programme, Phys. Sc, T145 (20111) 014001.
[15] L. Horton, et al., JET experiments with tritium and deuterium–tritium mixtures, Fus. Eng. Des 109-111 (2016) 925–936.
[16] J. Mailloux, et al., Overview of JET results for optimising ITER operation, Nucl. Fusion 62 (4) (2022) 042026.
[17] Z. Ghani, JET Neutron yield data (2QNZ84 v2.0), EUROfusion IDM, 2024.
[18] H. Sjöstrand, et al., Triton burn-up neutron emission in JET low current plasmas, J. Phys. D: Appl. Phys (41) (2008) 115208.
[19] The JET Operations Team (presented by D.B. King), JET machine operations in T&D-T, Nucl. Fusion 64 (2024) 106014. ?
[20] D. Flammini, Neutronic analyses for the equatorial diagnostic port plug #12 in ITER, Fus. Eng. Des 193 (2023) 113639.
[21] F. Brown, B. Kiedrowski, J. Bull, MCNP5-1.60 Release Notes LANL report LA-UR-10-06235 (2010).
[22] L. Bertalot, et al., Present Status of ITER Neutron Diagnostics Development, J. Fusion Energy 38 (2019) 283–290.
[23] P. Batistoni, et al., 14 MeV calibration of JET neutron detectors—phase 1: calibration and characterization of the neutron source, Nucl. Fusion 58 (2018) 026012.
[24] P. Batistoni, et al., 14 MeV calibration of JET neutron detectors—phase 2: in-vessel calibration, Nucl. Fusion 56 (2018) 106016.
[25] Z. Ghani, et al., Overview of DT Neutron Yield Calibrations at the JET Tokamak, in: DVCM meeting, 2024. Jan.
[26] L.W. Packer, et al., ITER materials irradiation within the D–T neutron environment at JET: post-irradiation radioactivity analysis following the DTE2 experimental campaign, Nucl. Fusion 64 (2024) 10.
[27] L.W. Packer, et al., Activation of ITER materials in JET: nuclear characterisation experiments for the long-term irradiation station, Nucl. Fusion 58 (2018) 096013.
[28] L.W. Packer, et al., Technological exploitation of the JET neutron environment: progress in ITER materials irradiation and nuclear analysis, Nucl. Fusion 61 (2021) 116057.
[29] M.I. Savva, et al., Application of VERDI detectors for neutron fluence measurements during the JET 2019 Deuterium-Deuterium campaign, Fus. Eng. Des 166 (2021) 112286.
[30] D.B. Pelowitz, et al., MCNP6 user's man. version 1 Alamos doc. number 0 (2013). LA-CP-13-00634 Rev.
[31] G. Schnabel, FENDL: libr. fusion res. appl. Nucl. Data Sheets 193 (2024) 1–78. February.
[32] J.C. Sublet, J.W. Eastwood, J.G. Morgan, FISPACT-II User Man. 11 (11 Issue 6) (2014). Technical Report CCFE-R.
[33] A. Trkov, et al., IRDFF-II: a new neutron metrology library Nucl, Data Sheets 163 (2020) 1–108.
[34] A.J.M. Plompen, O. Cabellos, C. De Saint Jean, et al., The joint evaluated fission and fusion nuclear data library, JEFF-3.3, Eur. Phys. J. A 56 (2020) 181.
[35] A.J. Koning, D. Rochman, Modern Nuclear Data Evaluation With The TALYS Code System, Nucl. Data Sheets 113 (2012) 2841.
[36] A. Wójcik-Gargula, et al., Evidence of silver impurities in irradiated Cu-based alloys and implications for the long-lived radioactive waste from ITER, submitted to Fus, Eng. Des. In Press.
[37] I. Lengar, et al., Radiation damage and nuclear heating studies in selected functional materials during the JET DT campaign, Fus, Eng, Des. 109-111 (2016) 1011–1015.
[38] L. Skuja, et al., Defects in oxide glasses, Phys. Status Solidi 2 (1) (2005) 15–24.
[39] S. Girard, et al., Radiation Effects on Silica-Based Optical Fibers: recent Advances and Future Challenges, IEEe Trans, Nucl, Sci 60 (3) (2013) 2015–2036.
[40] M. Angelone, et al., Performance test of radiation detectors developed for ITER-TBM, Fusion Eng, Des 136 (2018) 1386–1390.
[41] P. Batistoni, et al., Neutronics exp. helium cool. pebble bed (HCPB) breed. blanket mock-Fusion Eng, Des 82 (15–24) (2007) 2095–2104.
[42] N. Fonnesu, et al., Measurement of tritium production in the helium cooled pebble bed test blanket module mock-up at JET during DTE2, Eur, Phys, J. Plus 139 (2024) 893.
[43] R. Worral, et al., The development, testing and comparison of unfolding methods in SPECTRA-UF for neutron spectrometry, Fusion Eng, Des 161 (2020) 112038.
[44] C. Grove, et al., Neutron Spectrum Unfolding of Activation Foils Irradiated in JET's Deuterium-TritiumFusion Environment, presented at, in: IEEE NSS Conference, Tampa, Florida, USA, 2024, 26 Oct. –2 Nov.
[45] R. Villari, et al., Neutronics Experiments and Analyses in Preparation of DT Operations at JET, Fusion Eng. Des. 109-111 (2016) 895–905.
[46] R. Villari, et al., ITER oriented neutronics benchmark experiments on neutron streaming and shutdown dose rate at JET, Fus, Eng, Des 107 (2017) 171–176.
[47] R. Villari, et al., Shutdown Dose Rate neutronics experiment during high performances DD operations at JET, Fusion Eng. Des. 136 (2018) 1545–1549.
[48] N. Fonnesu, et al., The preparation of the Shutdown Dose Rate experiment for the next JET Deuterium-Tritium campaign, Fus, Eng, Des 123 (2017) 1039–1043. Nov.
[49] N. Fonnesu, et al., Shutdown Dose Rate Measurements after the 2016 Deuterium-Deuterium Campaign at JET, Fusion Eng. Des. 136 (2018) 1348–1353.
[50] N. Fonnesu, R. Villari, D. Flammini, P. Batistoni, U. Fischer, P. Pereslavtsev, Shutdown Dose Rate Studies for the DTE2 Campaign at JET, Fusion Eng. Des. 161 (2020) 112009.
[51] U. Fischer, et al., Review and validation of shutdown dose rate estimation techniques for application to ITER, Fusion Sci, Technol 64 (2013) 563–570.
[52] P. Batistoni, et al., Benchmark experiments on neutron streaming through JET Torus Hall penetrations, Nucl. Fusion 55 (2015) 053028.
[53] J. Naish, et al., Comparison of neutron flux streaming calculations to the 2019 JET Experimental Deuterium-Deuterium Results, Fusion Eng. Des. 170 (2021) 112538.
[54] B. Kos, et al., Application of ADVANTG to the JET3 - NEXP streaming benchmark experiment, Fus. Eng. Des 147 (2019) (2019) 111252.
[55] T. Vasilopoulou, et al., Activation foil measurements at JET in preparation for D-T plasma operation, Fus, Eng, Des 146 (2019) 250–255.
[56] B. Obryk, et al., TLD calibration at neutron field for JET fusion facility, Nucl. Inst, Methods Phys. Res. A 904 (2018) 202–213. Oct.
[57] T. Vasilopoulou, et al., Improved neutron activation dosimetry for fusion, Fus, Eng, Des 139 (2019) 109–114.
[58] C. Werner, J.S. Bull, MCNP Users Man. - Code Version 6.2 LA-UR-17-29981 (2017).
[59] S.W. Mosher, et al., Algorithmic Improvements to MCNP5 for High-Resolution Fusion Neutronics Analyses, Fusion Sci. Technol. 74 (4) (2018) 263–276.
[60] TRIPOLI-4, Project Team. TRIPOLI-4 version 8 User Guide, CEA-R-6316 (2013). Feb.
[61] I. Lengar, et al., Characterisation of the neutron field for streaming analyses in TT operations at JET, Fusion Eng. Des. 202 (2024) 114351.
[62] J.B. Pontier, et al., Simulation of the DD, TT and DT JET Neutron Streaming Experiments with TRIPOLI-4® Monte-Carlo code, in: EPJ Web Conf., Joint International Conference on Supercomputing in Nuclear Applications + Monte Carlo (SNA + MC 2024) 302, 2024 16005.
[63] P.K. Romano, et al., OpenMC: a state-of-the-art Monte Carlo code for research and development, Ann. Nucl. Energy 82 (2015) 90–97.
[64] N. Fonnesu, et al., Dose Rate Measurements During the Tritium Campaign at JET and Diagnostic Improvements for the Deuterium-Tritium Experiments, IEEE Trans. Plasma Sci. (2022) 1–7, https://doi.org/10.1109/TPS.2022.3169631.
[65] N. Fonnesu, et al., Shutdown Dose Rate experiment at JET during DTE2, Eur, Phys, J. Plus 139 (2024) 432.
[66] Y. Chen, U. Fischer, Rigorous MCNP based shutdown dose rate calculations: computational scheme verification calculations and application to ITER, Fusion Eng, Des 63–64 (2002) 107–114.
[67] A. Davis, R. Pampin, Benchmarking the MCR2S system for high-resolution activation dose analysis in ITER, Fusion Eng, Des 85 (2010) 87–92.
[68] T. Eade, et al., Shutdown dose rate benchmarking using modern particle transport codes, Nucl. Fusion 60 (2020) 056024.
[69] P. Sauvan, et al., Development of the R2SUNED Code System for Shutdown Dose Rate Calculations, IEEe Trans, Nucl, Sci 63 (1) (2016) 375–384, https://doi.org/10.1109/TNS.2015.2507138.
[70] P. Pereslatvsev, et al., Novel approach for efficient calculations of mesh based Monte Carlo shutdown dose rates and related V&V analyses on JET, Fusion Eng, Des 89 (2014) 2083–2087.
[71] D. Valenza, H. Iida, R. Plenteda, R.T. Santoro, Proposal of shutdown dose estimation method by Monte Carlo code, Fusion Eng. Des. 55 (4) (2001) 411–418.
[72] R. Villari, et al., Shutdown dose rate benchmark experiment at JET to validate the three-dimensional Advanced-D1S method, Fusion Eng. Des. 87 (2012) 1095–1100.
[73] R. Villari, et al., Shutdown dose rate assessment with the Advanced D1S method: development, applications and validation, Fusion Eng, Des 80 (2014) 2083–2087.
[74] R. Villari, et al., Development of the Advanced D1S for shutdown dose rate calculations in fusion reactors, Trans. Am. Nucl. Soc. Vol. 116 (2017) 255–258.

[75] G. Mariano, N.Fonnesu D.Flammini, F. Moro, R. Villari, Progress in development of advanced D1S dynamic code for three-dimensional shutdown dose rate calculations, Fusion Eng. Des. 157 (2020) 111631.
[76] P. Sauvan, et al., D1SUNED system for the determination of decay photon related quantities, Fusion Eng. Des. 151 (2020), https://doi.org/10.1016/j.fusengdes.2019.111399.
[77] G. Pedroche, P. Sauvan, J. Alguacil, J. Sanz, R. Ju, Nuclear data for D1SUNED for the study of ITER planned in-situ maintenance dose scenarios, Fusion Eng. Des. 170 (2021) 1–7, https://doi.org/10.1016/j.fusengdes.2021.112646.
[78] T. Eade, A new novel-1-step shutdown dose rate method combining benefits from the rigorous-2-step and direct-1-step methods, Fusion Eng. Des. 181 (2022) 113213.
[79] J. Sanz, O. Cabellos, and N. Garcia-Herranz, "ACAB Inventory code for nuclear applications: user's Manual V" 2008.
[80] B. Kos et al.: Compr. Anal. Streaming Shutdown Dose Rate Exp. JET ORNL Fusion Neutronics Work. Fusion Sci. Technol. vol 79, pp 284–304.
[81] I.C. GAULD, et al., Isotopic Depletion and Decay Methods and Analysis Capabilities in SCALE, Nucl, Technol 174 (2) (2011) 169.
[82] J. Alguacil, et al., Analysis of discrepancies between D1S and R2S results of 2016 DD JET Campaign, Nucl. Fusion 62 (9) (2022), https://doi.org/10.1088/1741-4326/ac7e5d art096015.
[83] A. Žohar, L. Snoj, On the dose fields due to activated cooling water in nuclear facilities, Prog. Nucl. Energy 117 (2019) 103042.
[84] R.T. Santoro, V. Khripunov, H. Iida, R.R. Parker, Radionuclide production in the ITER water coolant, in: 17th IEEE/NPSS Symposium Fusion Engineering (Cat. No.97CH36131), San Diego, CA, USA 1, 1997, pp. 137–140, https://doi.org/10.1109/FUSION.1997.687005.
[85] M. De Pietri J. Alguacil, A. Kolsek, G. Pedroche, N. Ghirelli, E. Polunovskiy, M. Loughlin, Y. Le Tonqueze, J. Sanz, R. Juarez, Integral modelling of the ITER cooling water systems radiation source for applications outside of the Bio-shield, Fusion Eng, Des 171 (2021) 112575.
[86] Z. Ghani, A. Turner, S. Mangham, J. Naish, M. Lis, L. Packer, M, Loughlin Radiation levels in the ITER tokamak complex during and after plasma operation, Fusion Eng. Des. 96–97 (2015) 261–264. VolumesOctober.
[87] M. Loughlin, M. Angelone, P. Batistoni, L. Bertalot, J. Eskhult, C. Konno, R. Pampin, A. Polevoi, E. Polunovskiy, Status and verification strategy for ITER neutronics, Fusion Eng. Des 89 (9–10) (2014) 1865–1869.
[88] Y. Uno, et al., Absolute measurement of D–T neutron flux with a monitor using activation of flowing water, Fusion Eng. Des. 56–57 (2001) 895–898.
[89] C.R. Nobs, et al., Computational evaluation of N-16 measurements for a 14 MeV neutron.irradiation of an ITER first wall component with water circuit, Fusion Eng. Des. 159 (2020).
[90] F. Andreoli, et al., Comparison between measurement and calculations for a 14 MeV neutron water activation experiment, in: EPJ Web of Conferences 239, EDP Sciences, 2020 21002.
[91] M. Angelone, et al., Measurement of delayed neutron emission from water activated by 14 MeV neutrons in a FW mock-up of ITER, Fusion Eng, Des 160 (2020) 111998.
[92] D. Kotnik, et al., Design optimization of the closed-water activation loop at the JSI irradiation facility, Fusion Eng. Des. 193 (2023) 113632.
[93] V. Radulovic, et al., Preparation of a water activation experiment at JET to support ITER, Fusion Eng. Des. 169 (2021) 112410.
[94] E. Lerche, et al., Long pulse oper. JET ITER-Wall.
[95] D. King, et al., in: Technical and Engineering challenges for long pulses on JET ITER Like Wall, 2nd Technical Meeting on Long Pulse Operation of Fusion Devices, IAEA Headquarters, Vienna, 2024, 14-18 Oct.
[96] T.A. Berry, et al., Integration of fluid dynamics into activation calculations for fusion, Fusion Eng. Des. 173 (2021) 112894.
[97] G.A. Spagnuolo, et al., A multi-physics integrated approach to breeding blanket modelling and design, Fusion Eng. Des. 143 (2019).
[98] P. Chiovaro, et al., Investigation of the DEMO WCLL Breeding Blanket Cooling Water Activation, Fusion Eng. Des. 157 (2020) 111697 article number.
[99] M. De Pietri, FLUNED code repos. (2023). https://github.com/marco-de-pietri/FLUNED-repository.
[100] MarcoDe Pietri, Javier Alguacil, Eduardo Rodríguez, Rafael Juárez, Development and validation in water of FLUNED, an open-source tool for fluid activation calculations, Comput, Phys, Commun 291 (2023) 108807.
[101] R. Pampin, F. Cau, M. Fabbri, J. Izquierdo, A. Portone, Improving the estimation of activation levels in flowing liquids under irradiation and decay, Nucl. Fusion 61 (2021) 036003.
[102] C. Moreno Carrero, F. Cau, R. Pampin, Radio-species transport model for coupled fluid dynamics-neutron activation calculations, Fusion Eng. Des. 181 (2022) 113171.
[103] J.L. Autran, S. Moindjie, D. Munteanu, M. Dentan, P. Moreau, et al., Real-Time Characterization of Neutron-Induced SEUs in Fusion Experiments at WEST Tokamak During D-D Plasma Operation, IEEe Trans, Nucl, Sci 69 (3) (2022) 501–511. March.
[104] M. Dentan, G. Borgese, J.L. Autran, D. Munteanu, S. Moindjie, et al., Preliminary Study of Electronics Reliability in ITER Neutron Environment, in: 22nd European Conference on Radiation and Its Effects on Components and Systems (RADECS), Venice, Italy, 2022, pp. 74–78, 3-7 Oct(ieeexplore 10412483.
[105] M. Dentan, M. Cecchetto, S. Moindjie, J.L. Autran, et al., Real-Time SER measurements of CMOS Bulk 40 nm and 65 nm SRAMs combined with neutron spectrometry at the JET Tokamak during D-D and D-T plasma operation, IEEe Trans, Nucl, Sci (2024) in press.
[106] S. Moindjie, D. Munteanu, J.L. Autran, M. Dentan, et al., Fusion Neutron-Induced Soft Errors During Long Pulse D-D Plasma Discharges in the WEST Tokamak, IEEe Trans, Nucl, Sci 71 (8) (2024) 1496–1502. Aug.
[107] M. Cecchetto, R.G. Alía, F. Wrobel, A. Coronetti, et al., 0.1–10 MeV Neutron Soft Error Rate in Accelerator and Atmospheric Environments, IEEe Trans, Nucl, Sci 68 (5) (2021) 873–883. May.
[108] M. Cecchetto, R. García Alía, F. Wrobel, M. Tali, O. Stein, et al., Thermal Neutron-Induced SEUs in the LHC Accelerator Environment, IEEe Trans, Nucl, Sci 67 (7) (2020) 1412–1420. July.